

Constraining grand-unified effective field theories: An $SO(10)$ example of radiative symmetry breaking

Aaron Held^{a,b} Jan Kwapisz^{c,d} Lohan Sartore^e

^a*Theoretisch-Physikalisches Institut, Friedrich-Schiller-Universität Jena, Max-Wien-Platz 1, 07743 Jena, Germany*

^b*The Princeton Gravity Initiative, Jadwin Hall, Princeton University, Princeton, New Jersey 08544, U.S.*

^c*Institute of Theoretical Physics, Faculty of Physics, University of Warsaw, ul. Pasteura 5, Warsaw, Poland*

^d*CP3-Origins, University of Southern Denmark, Campusvej 55, DK-5230 Odense M, Denmark*

^e*Laboratoire de Physique Subatomique et de Cosmologie, Université Grenoble-Alpes, CNRS/IN2P3, 53 Avenue des Martyrs, 38026 Grenoble, France*

E-mail: aaron.held@uni-jena.de, jkwapisz@fuw.edu.pl,
sartore@lpsc.in2p3.fr

ABSTRACT: Grand unified theories are very appealing both phenomenologically and theoretically. However, to realise the Standard Model at low energies, the unified symmetry group has to be partially broken in just the right way to obtain the Standard Model. We work in a minimal $SO(10)$ model with $\mathbf{16}_H$ and $\mathbf{45}_H$ scalar representations. We explicitly demonstrate that the requirement of successful radiative symmetry-breaking to the correct vacuum expectation value provides strong constraints on the underlying microscopic dynamics. Without assumptions about dynamics beyond the Planck scale, we find that the Planckian EFT parameter space can be significantly constrained by demanding a viable breaking chain to be realised radiatively.

Contents

1	Introduction	1
2	The blueprint: How to constrain grand-unified effective field theories	3
3	Methodology: RG-flow, effective potential, and breaking patterns	5
3.1	Renormalisation group-improved 1-loop potential	5
3.2	Minimisation of the RG-improved potential	8
3.3	Breaking patterns triggered by the RG-flow	10
4	The model: minimal SO(10)	11
4.1	SO(10) with fermionic $\mathbf{16}_F$, scalar $\mathbf{16}_H$ and $\mathbf{45}_H$	12
4.2	Potential breaking chains of the minimal SO(10) model	13
4.2.1	Admissible breaking patterns.	13
4.2.2	Non-admissible breaking patterns.	15
4.2.3	Non-observable broken phases	16
4.2.4	Viability of admissible breaking patterns	18
5	Results	20
5.1	Constraints from an SO(10) model with $\mathbf{45}_H$ scalar potential	21
5.2	Constraints from an SO(10) model with $\mathbf{16}_H \oplus \mathbf{45}_H$ scalar potential	24
6	Discussion	27
6.1	Summary of the main results	27
6.2	Comments on a link to three specific quantum-gravity scenarios	27
6.3	Outlook	30
A	One-loop RG-improved potential	32
A.1	Stationary point equation	32
A.2	RG-improvement and the Gildener-Weinberg approximation	34
A.3	Minimisation beyond the one-loop approximation	37
A.4	Numerical performance and accuracy of the minimisation procedure	38
B	General tree-level stability conditions	41
B.1	Stability of 2-vev vacuum manifolds	41
B.2	Stability of 3-vev vacuum manifolds	42
B.3	Stability violation for 3-vev manifolds	45
C	A quantitative measure of perturbativity	48

D	Scalar potential for the considered models	50
D.1	Definitions and conventions	50
D.2	Scalar potential for the $\mathbf{10}_H \oplus \mathbf{16}_H \oplus \mathbf{45}_H$ and $\mathbf{45}_H$ models	51
D.3	Scalar potential for the $\mathbf{16}_H \oplus \mathbf{45}_H$ model	51
E	β-functions	52
E.1	$\mathbf{10}_H \oplus \mathbf{16}_H \oplus \mathbf{45}_H$ model	52
E.2	$\mathbf{16}_H \oplus \mathbf{45}_H$ and $\mathbf{45}_H$ models	53

1 Introduction

Unification of the Standard Model (SM) gauge groups into a single grand unified theory (GUT) remains an attractive new-physics scenario: It has the potential to (i) provide an explanation for the seemingly coincidental near-equality of SM gauge couplings at the high-energy scale $M_{\text{GUT}} \sim 10^{15}$ GeV, see e.g. [1–3]; (ii) unify the apparent plethora of fermionic representations into a single GUT representation [4]; thereby (iii) account for heavy right-handed sterile neutrinos [5] with a suitable see-saw mechanism [5, 6]; and, in turn, (iv) offer a scenario for leptogenesis, see e.g. [7–9].

Yet the explanatory power of a GUT – manifest in relations among SM couplings – comes with the caveat of having to construct a viable mechanism to break the large gauge group in just the right way such as to retain the SM. Mirroring the successful Higgs-mechanism in the SM, the most common way to reduce the unified gauge group to the SM is via spontaneous symmetry breaking in a suitable scalar potential [5]. Most GUT analyses to date simply assume that all group-theoretically possible breaking chains can be realised by some – potentially contrived and complicated – scalar potential. Oftentimes, the latter is not explicitly specified. Indeed, such potentials remain largely arbitrary without specific knowledge about microscopic boundary conditions, for instance, at the Planck scale. As a result, the plethora of SM parameters is effectively traded for a plethora of admissible breaking potentials. In particular, currently viable GUTs require more free parameters than the SM itself¹. In contrast to the Yukawa and gauge couplings, the (quartic) couplings entering the GUT potential are not directly constrained by the experimental data.

Several quantum-gravity scenarios hold the promise to predict Planck-scale boundary conditions, both on the gauge-Yukawa sector and the scalar potential, for the asymptotic safety investigations, see e.g. [10, 11] and for the string theory ones, see e.g. [12–15]. Naturally, such a link would benefit GUT model builders and QG phenomenologists alike:

- GUTs would aid QG phenomenology: The requirement of viable initial conditions promises to indirectly constrain the landscape of possible QG scenarios.

¹In particular the minimal viable $SO(10)$ with $\mathbf{10}_H \oplus \mathbf{126}_H \oplus \mathbf{45}_H$ possess roughly 20 couplings in the scalar potential only [5].

- QG would aid GUT model building: Any predictive QG scenario will, in turn, predict/constrain the Planckian parameter space and thereby may exclude (i.e., be incompatible with) specific GUTs.

To build this link, progress on both ends is required: On the one hand, Planck-scale predictions of QG scenarios have to be solidified. On the other hand, viable Planck-scale initial conditions have to be carved out specifically.

In the present work, we focus on the GUT side of progress. In particular, we point out that the requirement of viable radiative symmetry breaking – or rather the absence of non-viable radiative symmetry breaking – places strong constraints on the underlying Planck-scale initial conditions.

To do so, we treat the GUT as an effective field theory (EFT). The respective grand-unified effective field theory (GUEFT) is fully specified by its symmetry group \mathcal{G}_{GUT} – including a local gauge group $\mathcal{G}_{\text{GUT}}^{(\text{local})}$ as well as potential additional global symmetries $\mathcal{G}_{\text{GUT}}^{(\text{global})}$ – and the set of fermionic as well as scalar representations \mathcal{F}_{GUT} and \mathcal{S}_{GUT} , respectively. The respective EFT action includes all possible symmetry invariants that can be constructed from the gauge and matter fields. The initial conditions for the couplings dressing these symmetry invariants specify an explicit realisation of the GUEFT.

We then assume that some (in-principle unknown) UV dynamics provides said initial conditions of the GUEFT at some ultraviolet (UV) scale. In the following, we attribute that scale to the Planck scale and hence the UV dynamics to QG. Still, the general framework presented here applies more widely.

Once the initial conditions are specified at the Planck scale M_{Pl} , the renormalisation group (RG) equations evolve each such realisation towards lower energies, in particular down to observable electroweak scale where (some of) the couplings need to be matched to experiment. Physically, the change of couplings describes the field-theoretical process of integrating out degrees of freedom at scale k . Formally, the RG flow is defined by the β -functions, i.e.,

$$\beta_{c_i} = k \frac{\partial}{\partial k} c_i . \quad (1.1)$$

Here, we focus solely on the perturbative regime. This allows us to make use of (i) the computational toolkit PyR@TE 3 [16] to determine the full set of perturbative β -functions and (ii) the well-developed perturbative techniques for multidimensional effective potentials [17] (see also [18]). We also mention that if (i) and (ii) can be realised in a non-perturbative RG scheme, the developed framework can, in principle, be extended. However, we leave such application and, in particular, the proper inclusion of gravitational fluctuations and thus any trans-Planckian dynamics at $k > M_{\text{Pl}}$ for future work.

In this perturbative GUEFT setup, we will analyse, in particular, the question of radiative symmetry breaking by use of a (more generally applicable) blueprint.

The paper is organized as follows. In Sec. 2, we present the abstract blueprint for how to place phenomenological constraints on the parameter space at M_{Pl} . In particular, our

blueprint encompasses a novel set of systematic constraints on a viable (perturbative) scalar potential. In the Sec 3, we review the required and previously mentioned (see (i) and (ii) in the paragraph above) perturbative techniques. In Sec. 4 we focus on a particular minimal $SO(10)$ model. We discuss the possible breaking chains, including those that lead to the SM (admissible) but also many that do not (non-admissible). In Sec. 5, we present the explicit results for said model. In particular, we demonstrate how the Planckian parameter space is constrained with each individual constraint in the blueprint. In Sec. 6, we close with a wider discussion of our results and an outlook on future work. In particular, we briefly comment on how to (i) extend our results to a GUEFT with a realistic Yukawa sector and (ii) eventually connect these to QG scenarios that may set the Planckian initial conditions. Several technical details are delegated into appendices. The full form of the beta functions is given in App. E.

2 The blueprint: How to constrain grand-unified effective field theories

The following section can be read in two ways: either as a physical description of the methodology applied to the specific $SO(10)$ models in this paper; or as a more general blueprint applicable to any grand-unified effective field theory (GUEFT).

We define a GUEFT by its symmetry group \mathcal{G}_{GUT} – including a local gauge group $\mathcal{G}_{\text{GUT}}^{(\text{local})}$ as well as potential additional global symmetries $\mathcal{G}_{\text{GUT}}^{(\text{global})}$ – and the set of fermionic as well as scalar representations \mathcal{F}_{GUT} and \mathcal{S}_{GUT} , respectively. For instance, the two models that we will investigate in Sec. 5 as an explicit example, are denoted by

$$\left\{ \mathcal{G}_{\text{GUT}}^{(\text{local})}, \mathcal{F}_{\text{GUT}}, \mathcal{S}_{\text{GUT}} \right\} = \left\{ \text{SO}(10), \mathbf{16}_F^{(i)}, \mathbf{45}_H \right\}, \quad (\text{see Sec. 5.1}) \quad (2.1)$$

$$\left\{ \mathcal{G}_{\text{GUT}}^{(\text{local})}, \mathcal{F}_{\text{GUT}}, \mathcal{S}_{\text{GUT}} \right\} = \left\{ \text{SO}(10), \mathbf{16}_F^{(i)}, \mathbf{16}_H \oplus \mathbf{45}_H \right\}. \quad (\text{see Sec. 5.2}) \quad (2.2)$$

Herein, $i = 1, 2, 3$ denotes a family index. The models at hand do not exhibit additional global symmetries.

The purpose of the following blueprint is to constrain the possibility that such a GUEFT is a UV extension of the SM. Note that we distinguish the notions of UV extension and UV completion. By UV extension of the SM, we refer to some high-energy EFT which contains the SM at lower scales. In particular, we do not demand that the UV extension itself is UV-complete, i.e., extends to arbitrarily high energies without developing pathologies. By UV completion of the SM, we refer to a UV extension which moreover is UV-complete.

In principle, the respective EFT action includes all possible symmetry invariants that can be constructed from the gauge and matter fields. For this work, however, we will focus only on the marginal couplings only. This amounts to restricting the EFT-analysis to the perturbative regime around the free fixed point. Close to the free fixed point, canonically irrelevant couplings will be power-law suppressed.

Moreover, we omit potentially sizeable mass terms. In the presence of mass terms, the following constraints have to be re-interpreted but are nevertheless of relevance for phenomenology. We comment on this at the very end of this section.

In consequence, the GUEFT is parameterised by the initial conditions of all its marginal couplings at an a priori unknown high-energy cutoff scale k_{cutoff} . In the following, we will tentatively identify the cutoff scale with the Planck scale, i.e., $k_{\text{cutoff}} = M_{\text{Pl}}$.

In this setup, we first focus on a set of constraints in the scalar sector. These arise from radiative symmetry breaking and are necessary but not sufficient for the GUEFT to be a UV extension of the SM.

- (I.a) We demand tree-level stability at $k = M_{\text{Pl}}$.
- (I.b) We demand the absence of Landau poles between the first symmetry-breaking scale M_{GUT} and $k = M_{\text{Pl}}$. (Alternatively, one may define a perturbativity criterion and demand that the GUEFT remains perturbative between M_{GUT} and $k = M_{\text{Pl}}$.)
- (I.c) We demand that the deepest vacuum expectation value (vev) induced by radiative symmetry breaking, is admissible, i.e., remains invariant under the Standard Model gauge group $\mathcal{G}_{\text{SM}} \subset \mathcal{G}_{\text{GUT}}^{(\text{local})}$.

Each of these necessary conditions may be applied on its own to constrain the set of initial conditions at $k = M_{\text{Pl}}$. Applying the constraints in the above order is most efficient as we will explicitly demonstrate in Sec. 5.

On top of these constraints on the scalar potential, one may apply more commonly addressed phenomenological constraints on the gauge-Yukawa sector [1]. More precisely:

- (II.a) We demand gauge unification and a sufficiently long lifetime of the proton to avoid experimental proton-decay bounds, cf [1] for previous work.
- (II.b) We demand a viable Yukawa sector. (realising a viable Yukawa sector is in itself a very non-trivial question [15, 19, 20].)

The necessary conditions (I) in the scalar sector and (II) in the gauge-Yukawa sector can, in principle, depend on each other². Ideally, one would thus want to include the gauge and Yukawa couplings in the set of random initial conditions and apply (I) and (II) simultaneously. Alternatively, we fix the gauge and Yukawa couplings to approximate phenomenological values, see [5, 19, 21, 22]. Subsequently, we verify that the constraints which we obtain from (I) are not significantly altered when varying initial conditions in the gauge-Yukawa sector.

²Interdependence of (I) and (II) occurs not only via higher-loop corrections. For instance, the gauge coupling will impact the radiative symmetry-breaking scale. At the same time, the symmetry-breaking scale will impact the RG flow of the gauge couplings, even at 1-loop order.

The above two sets of constraints can be viewed as necessary consistency constraints for a GUEFT to be a viable UV extension of the SM. In that sense, they realise a set of exclusion principles in a top-down approach to grand unification.

In addition, one may specify an underlying UV completion. This extends the GUEFT to arbitrarily high scales above $k = M_{\text{Pl}}$ and – within each specific UV-complete model – typically results in additional constraints.

- (III) Strong additional constraints may arise from demanding that the initial conditions can arise from a specific assumption about the transplanckian theory, i.e., from a specific model of or assumption about quantum gravity.

We discuss the significance of such constraints alongside existing literature as part of the conclusions in Sec. 6. An explicit implementation is left to future work.

As promised, we come back to the significance of sizeable scalar mass terms. Negative mass terms provide an independent mechanism for symmetry breaking in any otherwise stable potential. At the same time, mass terms are relevant couplings and thus entirely unconstrained in the perturbative range. Hence, we caution that the inclusion of mass terms can partially invalidate the the above constraints: In particular, initial conditions which are excluded because they break to a non-admissible vacuum, cf. (I.c), may actually be viable due to sizeable mass terms.

Two comments are in order. First, there is an intrinsic interest to studying models without bare mass terms. However, such arguments are oftentimes based on some notion of naturalness, for which we see no fundamental rationale.

Second, and more importantly, mass terms do not invalidate the radiative symmetry-breaking scale. For instance, assume that a specific realisation of a GUEFT radiatively breaks to a non-admissible vacuum at $M_{\text{GUT}}^{(\text{radiative})}$. An additional mass-term induced breaking scale $M_{\text{GUT}}^{(\text{mass})}$ may in principle break to an admissible vacuum. However, there remains a constraint that this potentially viable breaking has to then occur at $M_{\text{GUT}}^{(\text{mass})} > M_{\text{GUT}}^{(\text{radiative})}$. In turn any such $M_{\text{GUT}}^{(\text{mass})} > M_{\text{GUT}}^{(\text{radiative})}$ may be in conflict with other observational constraints such as the ones on the gauge-Yukawa sector, cf. (II) above.

Nevertheless, we think that the inclusion of mass terms poses an important future extension of our work.

3 Methodology: RG-flow, effective potential, and breaking patterns

3.1 Renormalisation group-improved 1-loop potential

In this work we are interested in the radiative minima of the potential generated due to the renormalisation group flow of the quartic couplings. Hence the renormalisation group equations (RGEs) constitute the principal tool in our analysis. The schematic form of the one-loop RGEs are given in the seminal papers [23–25], see also the recent discussion [26–28].

In absence of mass terms in the tree-level potential, any non trivial minimum must be generated by higher order corrections to the scalar potential. The dependence of loop corrections on the arbitrary renormalisation scale can be alleviated using techniques of RG-improvement of the scalar potential. Such techniques generally allow for a better approximation of the all-order quantum potential, already in the one-loop truncation. For these reasons, we have used in this work the RG-improved 1-loop potential to study the breaking patterns of a GUT model, in a formalism that we now briefly review.

Considering a gauge theory with a scalar multiplet noted ϕ , and using the conventions of [17], the one-loop contributions to the effective potential can be put in the form

$$V^{(1)} = \mathbb{A} + \mathbb{B} \log \frac{\varphi^2}{\mu_0^2} \quad (3.1)$$

where μ_0 is the arbitrary renormalisation scale and where $\varphi = \sqrt{\phi_i \phi^i}$. The quantities \mathbb{A} and \mathbb{B} receive contributions from the scalar, gauge and Yukawa sectors of the theory. In the $\overline{\text{MS}}$ scheme and working in the Landau gauge, they may be expressed as

$$\mathbb{A} = \frac{1}{64\pi^2} \sum_{i=s,g,f} n_i \text{Tr} \left[M_i^4 \left(\log \frac{M_i^2}{\varphi^2} - C_i \right) \right], \quad (3.2)$$

$$\mathbb{B} = \frac{1}{64\pi^2} \sum_{i=s,g,f} n_i \text{Tr} (M_i^4). \quad (3.3)$$

where the numerical constants n_i and C_i take the values

$$\begin{aligned} n_s &= 1, & n_g &= 3, & n_f &= -2, \\ C_s &= \frac{3}{2}, & C_g &= \frac{5}{6}, & C_f &= \frac{3}{2}, \end{aligned} \quad (3.4)$$

and where $M_{s,g,f}$ respectively stand for the field-dependent mass matrices of the scalars, gauge bosons and fermions of the model. The first two matrices can be straightforwardly computed once the scalar potential and the gauge generators of the scalar representations have been fixed:

$$(M_s^2)_{ij} = \frac{\partial^2 V^{(0)}}{\partial \phi^i \partial \phi^j} \quad (3.5)$$

$$(M_g^2)_{AB} = g^2 \{T_A, T_B\}_{ij} \phi^i \phi^j \quad (3.6)$$

The $\mathbf{45}_H$ and $\mathbf{16}_H \oplus \mathbf{45}_H$ models considered in this work contain no Yukawa interactions, hence the M_f mass matrix will be taken to vanish.

The dependence of $V^{(1)}$ on the renormalisation scale μ_0 is an artifact of working at fixed order in perturbation theory, and introduces arbitrariness in the computations. In some circumstances, simple prescriptions on the value of μ_0 may be given that are appropriate for computations involving the quantum potential. Such prescriptions are in particular suitable for single-scale models, thus giving a reasonable approximation of the effective potential around this one scale. For computations involving a wider range of energy scales,

or in theories with multiple characteristic scales (*e.g.* several vevs and/or masses, possibly spanning over orders of magnitude), one inevitably encounters large logarithms. Various renormalisation group techniques were developed to resum such large logarithms (see *e.g.* [29–36]), with the aim of yielding a well-behaved quantum potential for multi-scale theories and/or over large energy ranges. Such a procedure is generally referred to as renormalisation group improvement of the scalar potential.

The $SO(10)$ model considered in this work (and generally any GUT model) enters in the category of multi-scale theories, requiring an appropriate procedure of RG-improvement. Here we briefly review the method developed in [17] and further extended in [18] in the case of classically scale invariant potentials. The starting point is to consider the Callan-Symanzik equation satisfied by the all-order quantum potential, stating that the total derivative of the effective potential with respect to the renormalisation scale vanishes:

$$\frac{dV^{\text{eff}}}{d \log \mu_0} = \left(\frac{\partial}{\partial \log \mu_0} + \sum_i \beta(g_i) \frac{\partial}{\partial g_i} - \phi^i \gamma^{ij} \frac{\partial}{\partial \phi^j} \right) V^{\text{eff}} = 0. \quad (3.7)$$

The above relation describes the invariance of the quantum potential on the renormalisation scale, given that the couplings of the theory are evolved according to their β -functions, and the field strength renormalisation values according to their anomalous dimension matrix γ . Following [17, 18] and using (3.7), we may simultaneously promote the RG-scale μ_0 to a field-dependent quantity $\mu(\phi^i)$, and the couplings and fields to μ -dependent quantities. Formally, we have

$$\begin{aligned} \mu_0 &\longrightarrow \mu(\phi^i), \\ \lambda &\longrightarrow \lambda(\mu(\phi^i)), \\ \phi &\longrightarrow \phi(\mu(\phi^i)). \end{aligned} \quad (3.8)$$

The cornerstone of the RG-improvement procedure presented in [17] is to note that for each point in the field space, and as long as perturbation theory holds, there exists a renormalisation scale μ_* such that the one-loop corrections $V^{(1)}$ vanish³:

$$V^{(1)}(\phi^i, \lambda^i; \mu_*) = \mathbb{A}(\phi^i(\mu_*), \lambda^i(\mu_*)) + \mathbb{B}(\phi^i(\mu_*), \lambda^i(\mu_*)) \log \frac{\varphi^2}{\mu_*^2} = 0. \quad (3.9)$$

The above relation gives the implicit definition of the field-dependent scale $\mu_*(\phi^i)$, and is shown in [17] to allow for a resummation of a certain class of logarithmic contributions. Going on, the full 1-loop effective potential is simply given by its tree-level contribution, with the couplings and fields are evaluated at the scale μ_* :

$$V^{\text{eff}}(\phi^i) = V^{(0)}(\phi^i; \mu_*(\phi^i)). \quad (3.10)$$

That the RG-improved effective potential takes its tree-level form provides valuable insight on the conditions of radiative symmetry breaking in classically scale-invariant models [17, 18, 37].

³In presence of negative eigenvalues in the mass matrices, one may instead require the real part of the one-loop corrections to vanish.

In particular, a necessary condition for symmetry breaking to occur is that the tree-level stability conditions of the scalar potential must be violated at some scale along the RG-flow. As illustrated in the next sections, this observation crucially allows to determine whether the breaking of the $SO(10)$ symmetry towards a specific subgroup will happen at all, given some initial conditions for the quartic couplings at the high energy scale.

3.2 Minimisation of the RG-improved potential

In order to identify the breaking patterns of the model, one needs to evaluate the depth of the RG-improved potential at the minimum for each relevant vacuum configuration. The set of stationary point equations of the RG-improved potential are derived in App. A, and would in principle need to be solved numerically in order to determine the position of its global minimum. Such a numerical minimisation procedure, however, can be computationally very costly and therefore rather inappropriate in the context of this work, where a scan over a large number of points is to be performed. Instead, we propose in this section a simple procedure allowing to estimate (rather accurately) the position and depth of the minimum of the RG-improved potential.

In App. A, we derive the radial stationary point equation (A.9) satisfied by the RG-improved potential at a minimum, in the $\mathcal{O}(\hbar)$ approximation:

$$4V^{\text{eff}} + 2\mathbb{B} = 0, \quad \frac{d\mathbb{A}}{dt} \approx 0 \quad \text{and} \quad \frac{d\mathbb{B}}{dt} \approx 0. \quad (3.11)$$

As mentioned in App. A.1, the quantity \mathbb{B} must be strictly positive at a minimum, thus implying

$$V^{\text{eff}} < 0. \quad (3.12)$$

Recalling that for all field values, V^{eff} takes its classically scale invariant tree-level form, this means in turn that the tree-level stability conditions must not hold at the RG-scale μ_*^{min} , defined such that

$$\frac{\partial V^{\text{eff}}}{\partial \langle \phi \rangle^i} \left(\langle \phi \rangle^i; \mu_*^{\text{min}} \left(\langle \phi \rangle^i \right) \right) = 0 \quad \text{and} \quad V^{(1)} \left(\langle \phi \rangle^i; \mu_*^{\text{min}} \left(\langle \phi \rangle^i \right) \right) = 0. \quad (3.13)$$

More concretely, μ_*^{min} is the value of the RG-improved scale μ_* evaluated at the vacuum $\langle \phi \rangle$. Letting μ_0 be some arbitrary high scale at which the tree-level potential is assumed to be stable, one can identify a scale μ_{GW} characterising the breaking of tree-level stability, such that

$$\mu_*^{\text{min}} < \mu_{\text{GW}} < \mu_0. \quad (3.14)$$

Hence at the RG-scale μ_{GW} the tree-level potential (without RG-improvement) develops flat directions, along which a minimum will be radiatively generated through the Gildener-Weinberg mechanism [38], see also App. A.2. A first important observation is that μ_{GW} gives an upper bound on the value of μ_* at the minimum, as well as a rough estimate of it.

This bound may be further refined observing that an additional scale $\tilde{\mu}$ can be identified, at which the quantity $\tilde{V}^{(0)}$ defined as

$$\tilde{V}^{(0)} \equiv V^{\text{eff}} + \frac{1}{2}\mathbb{B} \quad (3.15)$$

develops flat directions, see App. A. Since $\mathbb{B} > 0$ near the minimum, one has

$$\mu_*^{\text{min}} < \tilde{\mu} < \mu_{\text{GW}}, \quad (3.16)$$

so $\tilde{\mu}$ provides an improved upper bound for μ_*^{min} . In practice, the former scale provides in most cases a remarkably accurate estimation of μ_*^{min} , for reasons detailed and exemplified in Appendix A. Based on this observation, we have used for the purposes of the present analysis a simplified procedure to identify and characterise the minima of RG-improved potentials in an algorithmic fast and efficient way — the only other alternative being the minimisation via numerical methods, increasingly costly for vacuum structures with many vevs. For a given vacuum configuration, this minimisation procedure may be summarised as follows:

1. Starting with random values for the quartic couplings at some high scale μ_0 , the stability of the tree-level potential is asserted and unstable configurations are discarded.
2. Evolution of the quartic couplings according to their one-loop β -functions is performed down to some lower scale μ_1 . A natural choice for this scale is $\mu_1 \approx 10^{11}$ GeV, where the gauge coupling usually runs into a Landau pole⁴.
3. The scale $\tilde{\mu}$ at which $\tilde{V}^{(0)}$ develops flat directions is identified. To determine it in practice, one only needs to assert the tree-level stability conditions at each integration step over the considered energy range.
4. At the scale $\tilde{\mu}$, depending on the considered vacuum structure, the flat direction \vec{n} is identified (see Appendix (B)). Along this flat direction, the field values take the form

$$\phi = \varphi \vec{n} \quad (3.17)$$

5. The unique value of $\langle \varphi \rangle$ such that

$$V^{(1)}(\langle \varphi \rangle \vec{n}; \tilde{\mu}) = 0 \quad (3.18)$$

is identified. The field vector $\langle \phi \rangle = \langle \varphi \rangle \vec{n}$ constitutes an estimation of the exact position of the minimum.

6. Finally, the depth of the RG-improved potential at the minimum, *i.e.* the quantity

$$V^{\text{eff}}(\langle \phi \rangle) = V^{(0)}(\langle \phi \rangle; \tilde{\mu}) \quad (3.19)$$

is evaluated.

⁴The precise value of μ_1 is anyways rather arbitrary, since in practice one observes either the breakdown of $SO(10)$ or the occurrence of Landau poles along the way from μ_0 down to μ_1 .

In this form, the above procedure is essentially equivalent to a Gildener-Weinberg minimisation (see App. A.2). However, as explained in App. A.3, it can be straightforwardly extended to include $\mathcal{O}(\hbar^2)$ corrections characteristic of the 1-loop RG-improvement procedure. The accuracy of this procedure compared to a full-fledged numerical minimisation of the RG-improved potential is studied in Appendix A.4. From an algorithmic point of view, our method proves remarkably more efficient, in particular for multidimensional vacuum manifolds. The reason is rather simple: Here, one avoids the numerical minimisation of a multivariate function, whose evaluation at a point $\phi \in \mathbb{R}^N$ is itself rather costly (evaluating the potential at some given field value involves a root-finding algorithm to determine the RG-improved scale μ_*). Instead, two 1-dimensional numerical scans are performed, respectively to find the value of $\tilde{\mu}$ at step 3, then the value of $\langle\varphi\rangle$ at step 5.

3.3 Breaking patterns triggered by the RG-flow

As stated above, the spontaneous breakdown of $SO(10)$ — *i.e.* the occurrence of a non-trivial minimum of the RG-improved potential — is triggered around the RG-scale at which the tree-level potential turns unstable. While the knowledge of necessary stability conditions allows to discard points from the parameter space for which the scalar potential is clearly unstable (see step 1. in the minimisation procedure described above), the determination of the breaking patterns of the model requires additional information. In particular, given some vacuum manifold, there are in general several qualitatively different ways of violating the stability conditions (see App. B). When the RG-improved potential develops a non-trivial minimum, the resulting pattern of symmetry breaking depends in fact on the way the stability conditions get violated along the RG flow. More precisely, the set of stability conditions for a given vacuum structure can in general be expressed as the conjunction of n individual constraints:

$$S = S_1 \wedge \cdots \wedge S_n. \quad (3.20)$$

Defining \bar{S} as the condition of an unstable potential, one clearly has

$$\bar{S} = \bar{S}_1 \vee \cdots \vee \bar{S}_n, \quad (3.21)$$

and therefore the violation of any one of the S_i will trigger spontaneous symmetry breaking, in general towards different subgroups of original symmetry group. To illustrate this rather general statement, let us consider a concrete example. Namely, for the $\mathbf{16} \oplus \mathbf{45}$ $SO(10)$ model considered in the next section, a possible vacuum configuration leading to a $SU(5)$ breaking is obtained from Eq. (4.7) in the limit $\omega_R = \omega_B = \omega/\sqrt{5}$, $\chi_R = 0$

$$\langle V \rangle_{SU(5)} = \left(\lambda_1 + \frac{13}{20} \lambda_2 \right) \omega^4 + \left(2\lambda_8 + \frac{5}{2} \lambda_9 \right) \omega^2 \chi^2 + \lambda_6 \chi^4, \quad (3.22)$$

and matches the definition of a general 2-vev vacuum manifold given in Appendix B. Directly using the results from this appendix, we derive the following tree-level stability conditions⁵:

$$S_1 : \lambda_1 + \frac{13}{20}\lambda_2 > 0, \quad (3.23)$$

$$S_2 : \lambda_6 > 0, \quad (3.24)$$

$$S_3 : 2\lambda_8 + \frac{5}{2}\lambda_9 + 2\sqrt{\lambda_6 \left(\lambda_1 + \frac{13}{20}\lambda_2 \right)} > 0. \quad (3.25)$$

With these definitions at hand, the sufficient and necessary stability condition for this vacuum manifold is given by

$$S = S_1 \wedge S_2 \wedge S_3. \quad (3.26)$$

We note in passing that (3.26) only constitutes a set of necessary conditions for the stability of the full $SO(10)$ potential. Starting at a RG-scale μ_0 where S holds, spontaneous symmetry breaking will occur around the scale $\mu_{\text{GW}} < \mu_0$ at which any one of the S_i gets violated. This can occur in three distinct manners, generating in each case different vacuum configurations along the flat directions appearing at μ_{GW} :

$$\bar{S}_1 : \lambda_1(\mu_{\text{GW}}) + \frac{13}{20}\lambda_2(\mu_{\text{GW}}) = 0 \quad \rightarrow (\omega, \chi) = (\langle \omega \rangle, 0) \quad (3.27)$$

$$\bar{S}_2 : \lambda_6(\mu_{\text{GW}}) = 0 \quad \rightarrow (\omega, \chi) = (0, \langle \chi \rangle) \quad (3.28)$$

$$\bar{S}_3 : \left[2\lambda_8 + \frac{5}{2}\lambda_9 + 2\sqrt{\lambda_6 \left(\lambda_1 + \frac{13}{20}\lambda_2 \right)} \right] (\mu_{\text{GW}}) = 0 \quad \rightarrow (\omega, \chi) = (\langle \omega \rangle, \lambda \langle \omega \rangle) \quad (3.29)$$

Finally, based on group theoretical arguments, the residual symmetry group can be determined for each vacuum configuration. Here, \bar{S}_2 and \bar{S}_3 do generate a $SU(5)$ minimum, although in the former case ω vanishes. In contrast, the minimum associated with \bar{S}_1 preserves an additional $U(1)$ gauge factor, so the residual symmetry group is $SU(5) \times U(1)$.

The above example shows how to determine the residual gauge symmetry associated with a flat direction of the tree-level potential in a specific vacuum configuration. In addition, one must be able to determine the location and depth of the minimum of the effective potential. For this purpose, the procedure described in the previous section can be used in practice, allowing to estimate the position and depth of the minimum based on the study of the flat directions of \tilde{V}_0 . Such a procedure is reiterated for every relevant vacuum configuration, so that a deepest minimum can be identified. The corresponding residual symmetry gives the only allowed breaking pattern among the various subgroups initially identified.

4 The model: minimal $SO(10)$

In this section, we present the specific $SO(10)$ -GUT model to be investigated. After constructing the corresponding tree-level scalar potential, we establish a (non-exhaustive)

⁵It is implicitly understood that in the definition of S_3 , S_1 and S_2 must be satisfied.

classification of the possible breaking patterns of the model, clarifying in passing the distinction between the standard and flipped embeddings of the Standard Model into $SU(5) \times U(1) \subset SO(10)$. Our classification includes breaking patterns towards subgroups of $SO(10)$ that do not contain the Standard Model gauge group, allowing us in Sec. 5 to establish a novel kind of theoretical constraints on the parameters of the scalar sector. Finally, we comment on the property of some of breaking patterns to never occur (at least at tree-level) despite being allowed by the group-theoretical structure of the model.

4.1 $SO(10)$ with fermionic $\mathbf{16}_F$, scalar $\mathbf{16}_H$ and $\mathbf{45}_H$

For the $SO(10)$ -GUT the fermionic content of the Standard Model (together with right handed neutrinos) nicely fits into one, unifying $\mathbf{16}_F$ spinor representation. The minimal scalar content to reproduce the Standard Model electroweak theory is $\mathbf{16}_H \oplus \mathbf{45}_H$. In terms of its group-theoretical specification, the model reads

$$(\mathcal{G}_{\text{GUT}}, \mathcal{F}_{\text{GUT}}, \mathcal{S}_{\text{GUT}}) = (SO(10), \mathbf{16}_F, \mathbf{16}_H \oplus \mathbf{45}_H), \quad (4.1)$$

The Lagrangian is given by

$$\mathcal{L} = \mathcal{L}_K - V, \quad (4.2)$$

where the \mathcal{L}_K is the fermionic, scalar and gauge kinetic part and V is the $\mathbf{16}_H \oplus \mathbf{45}_H$ potential. Additionally, in order to break the electroweak symmetry a real $\mathbf{10}_H$ representation is introduced. In this case, a Yukawa interaction of the form $\mathbf{16}_F \mathbf{10}_H \mathbf{16}_F$ must be included and the Lagrangian reads

$$\mathcal{L} = \mathcal{L}_K + \mathcal{L}_Y - V. \quad (4.3)$$

We give in App. D a possible parameterisation of the most general scalar potential (and of \mathcal{L}_Y) including scalar representations $\mathbf{10}_H \oplus \mathbf{16}_H \oplus \mathbf{45}_H$. It should be stressed that the model hence obtained fails to produce a viable (*i.e.* SM-like) fermion sector at low energies for the simple reason that the single Yukawa matrix characterising the $\mathbf{16}_F \mathbf{10}_H \mathbf{16}_F$ interaction can always be diagonalised by a redefinition of the fermion fields. The question of constructing a minimal viable $SO(10)$ Yukawa sector has been largely addressed in the literature [] and will not be discussed here in detail. Nevertheless, we would like to mention that one promising model in that regard consists of a $\mathbf{10}_H \oplus \mathbf{45}_H \oplus \mathbf{126}_H$ scalar sector and shares features with the $\mathbf{10}_H \oplus \mathbf{16}_H \oplus \mathbf{45}_H$ model considered here, hence justifying one's motivations to investigate its main features despite its non-viable low-energy phenomenology⁶. In the present work, we will further simplify the overall picture by omitting the $\mathbf{10}_H$ representation and investigate models based on the scalar representations $\mathbf{16}_H \oplus \mathbf{45}_H$ and $\mathbf{45}_H$, respectively.

⁶On more pragmatic grounds, we should perhaps mention that the study of the scalar potential of the $\mathbf{10}_H \oplus \mathbf{45}_H \oplus \mathbf{126}_H$ model is anyways a challenging task due to the large number of gauge invariants (and hence of scalar couplings) which can be constructed.

In the former case, the tree-level scalar potential reduces to

$$V(\chi, \phi) = \frac{\lambda_1}{4} \text{Tr}(\Phi_{16}^2)^2 + \lambda_2 \text{Tr}(\Phi_{16}^4) + 4\lambda_6 (\chi^\dagger \chi)^2 + \lambda_7 (\chi_+^\dagger \Gamma_i \chi_-) (\chi_-^\dagger \Gamma^i \chi_+) + 2\lambda_8 (\chi^\dagger \chi) \text{Tr}(\Phi_{16}^2) + 8\lambda_9 \chi^\dagger \Phi_{16}^2 \chi. \quad (4.4)$$

where χ and ϕ respectively denote the $\mathbf{16}_H$ and $\mathbf{45}_H$ multiplets, and where all other relevant quantities were defined in App. D.

A series of articles in the early 1980's studying the $\mathbf{45}_H \oplus \mathbf{16}_H$ model [39–42] pointed that the only potentially viable minima of the (tree-level) potential induce a breaking towards either $SU(5) \times U(1)$ (which require large threshold corrections to be consistent with gauge-coupling unification [19]) or the excluded standard $SU(5)$. The other possible vacuum configurations in the Pati-Salam directions (see below for more detail) are not minima of the potential but saddle points. For this reason, the model has been disregarded for 30 years. However, models featuring a $\mathbf{45}_H$ have been recently revived in [5] by showing that one-loop quantum corrections to the potential could turn the phenomenologically preferable saddle points into actual minima. This observation further motivates the inclusion of quantum corrections to the scalar potential based on the formalism introduced in the previous section.

4.2 Potential breaking chains of the minimal $SO(10)$ model

A comprehensive discussion of symmetry breaking in the minimal $SO(10)$ model introduced above would require one to classify *all* potential breaking directions allowed by group-theoretical considerations. Here we study a subset of possible breaking patterns, yet considerably bigger than usually studied in the literature. This includes several breaking chains towards the Standard Model (in fact, all of the potentially viable ones) as well as non-viable vacuum configurations that break the $SO(10)$ towards non-SM directions. As will become clear later, the inclusion of additional non-viable breaking patterns can only tighten the constraints and further reduce the viable Planckian parameter space.

4.2.1 Admissible breaking patterns.

Following [22, 43], we observe that in order to break $SO(10)$ towards the Standard Model, the adjoint field $\mathbf{45}_H$ must have, up to arbitrary gauge transformations, the following vev texture:

$$\phi_{ij} = \text{Antidiag} \left(\omega_R, \omega_R, \omega_B, \omega_B, \omega_B, -\omega_B, -\omega_B, -\omega_B, -\omega_R, -\omega_R \right), \quad (4.5)$$

where $\sqrt{3}\omega_B$ and $\sqrt{2}\omega_R$ respectively stand for the vevs of the $(\mathbf{1}, \mathbf{1}, \mathbf{1}, 0)$ singlet and of the $(\mathbf{1}, \mathbf{1}, \mathbf{3}, 0)$ triplet contained in $\mathbf{45}_H$, according to a $3_C 2_L 2_R 1_{B-L}$ labelling convention. The above vev structure generally corresponds to a breaking towards $3_C 2_L 1_R 1_{B-L}$, and different

breaking chains can be conveniently recovered as particular cases:

$$\begin{aligned}\omega_R = 0 : & \quad SO(10) \longrightarrow 3_C 2_L 2_R 1_{B-L}, \\ \omega_B = 0 : & \quad SO(10) \longrightarrow 4_C 2_L 1_R, \\ \omega_R = \omega_B = \omega_5 : & \quad SO(10) \longrightarrow SU(5) \times U(1)_X.\end{aligned}$$

As compared to [22, 43], the *standard* and *flipped* $SU(5)$ configurations are not distinguished at the level of the first breaking stage. The main reason is that these two breaking chains are characterised by a different embedding of the SM gauge group within $SU(5) \times U(1)_X$, independently of the embedding of $SU(5) \times U(1)_X$ within $SO(10)$ (which is essentially unique). In practice, in the case where $\omega_R = -\omega_B$ (identified in [22, 43] as the flipped $SU(5)$ vacuum structure), one can always perform a gauge transformation effectively leading to $\omega_R \rightarrow -\omega_R$, and hence to $\omega_B = \omega_R$. Of course, such a transformation also affects the other scalar multiplets, and in particular $\mathbf{16}_H$. This will be discussed in more detail in what follows.

We now turn to the vev structure of $\mathbf{16}_H$. In addition to the vev of the $(\mathbf{1}, \mathbf{1}, \mathbf{2}, +\frac{1}{2})$ doublet, noted χ_R , we also consider a possibly non vanishing vev for the $(\mathbf{1}, -5)$ singlet under $SU(5) \times U(1)_X$, noted χ_5 . In the language of $3_C 2_L 2_R 1_{B-L}$ multiplets, introducing this additional vev, χ_5 , simply amounts to allowing for two SM vevs in the $(\mathbf{1}, \mathbf{1}, \mathbf{2}, +\frac{1}{2})$ doublet. With these notations, and in a gauge where the adjoint field has the vev structure (4.5), the scalar 16-plet can be put in the form⁷:

$$\chi = \frac{1}{\sqrt{2}} \left(0, -i\chi_5, 0, -\chi_R, 0, \chi_R, 0, i\chi_5, 0, \chi_5, 0, -i\chi_R, 0, -i\chi_R, 0, \chi_5 \right)^T. \quad (4.6)$$

Injecting (4.5) and (4.6) into the expression of the scalar potential at tree-level, we find:

$$\begin{aligned}\langle V \rangle = & \lambda_1 (3\omega_B^2 + 2\omega_R^2)^2 + \frac{\lambda_2}{4} (21\omega_B^4 + 36\omega_B^2\omega_R^2 + 8\omega_R^4) + 4\lambda_6 (|\chi_R|^2 + |\chi_5|^2)^2 \\ & + 4\lambda_8 (|\chi_R|^2 + |\chi_5|^2) (3\omega_B^2 + 2\omega_R^2) + \lambda_9 \left(|\chi_R|^2 (3\omega_B - 2\omega_R)^2 + |\chi_5|^2 (3\omega_B + 2\omega_R)^2 \right)\end{aligned} \quad (4.7)$$

The above expression makes it clear that the vacuum structure of the $\mathbf{16}_H$ multiplet will trigger the breaking towards the SM gauge group as follows:

$$\begin{aligned}\chi_R = 0, \chi_5 \neq 0 : & \quad SO(10) \longrightarrow SU(5) \times U(1)_X \longrightarrow SU(5) \longrightarrow \mathcal{G}_{\text{SM}}, \quad (\textit{standard}) \\ \chi_R \neq 0, \chi_5 = 0 : & \quad SO(10) \longrightarrow SU(5) \times U(1)_X \longrightarrow \mathcal{G}_{\text{SM}}. \quad (\textit{flipped})\end{aligned}$$

In the latter case, namely the flipped configuration, one exactly recovers the vacuum structure described in [22, 43] in a situation where $\omega_R = -\omega_B$. In the present approach, we instead consider that both embeddings of $SU(5)$ and $SU(5) \times U(1)_X$ in $SO(10)$ are characterised by the relation $\omega_R = \omega_B$. As stated previously, the latter relation can be recovered from the former making use of a class of gauge transformations effectively leading to

$$\omega_R \longleftrightarrow -\omega_R, \quad |\chi_R| \longleftrightarrow |\chi_5|. \quad (4.8)$$

⁷This form is only unique up to gauge transformations preserving the vev structure of $\mathbf{45}_H$.

We insist that the two approaches are equivalent in practice. However, we believe that the present description is conceptually more appealing since it emphasises that the *standard* and *flipped* configurations are only triggered during the second breaking step (towards the SM gauge group) and are therefore independent of the embedding of $SU(5) \times U(1)_X$ into $SO(10)$. Further, the existence of $SO(10)$ gauge transformations (4.8) has interesting implications regarding the physical occurrence of the standard and flipped SM embeddings. Namely, the gauge generators leading to (4.8) are clearly broken in any one of the SM vacua. Hence at a minimum they are associated with Goldstone modes, so both minima belong to a larger, continuous set of degenerate minima (*i.e.* to the same gauge orbit). Therefore, considering that the breaking towards the SM occurs at once – *i.e.* corresponds to a one-step breaking – the standard and flipped embeddings are formally equivalent. The degeneracy will however be removed if a large hierarchy exists among the vevs, allowing to adopt an effective description of the theory based on either $SU(5)$ or $SU(5) \times U(1)$ over a given energy range. Concretely, if $\chi_5 \gg \omega_R, \omega_B$ (or equivalently $\chi_R \gg \omega_R, \omega_B$), a first breaking towards $SU(5)$ is triggered at the GUT scale M_{GUT} , and the breaking towards the SM will be assumed to occur at an intermediate scale $M_I \ll M_{\text{GUT}}$. This case obviously corresponds to a standard embedding, since no $U(1)$ factor can enter in the definition of the hypercharge generator. Conversely, a first breaking can occur at M_{GUT} towards $SU(5) \times U(1)$, with a subsequent breaking towards the SM occurring at the lower scale M_I . In this case, one can expect that the precise form of the scalar potential in the $SU(5) \times U(1)$ phase will determine whether the SM embedding is standard or flipped, since RG-running effects in the $SU(5) \times U(1)$ phase would have spoiled the $SO(10)$ invariance of the vacuum manifold and therefore removed the degeneracy of the minima.

4.2.2 Non-admissible breaking patterns.

In addition to admissible breaking patterns, *i.e.* involving intermediate gauge groups which contain the SM, it is instructive to also consider any symmetry breaking towards other gauge groups. Doing so, one should be able to identify and exclude some regions of the parameter space that specifically trigger such breaking patterns. In particular, for the $\mathbf{16}_H \oplus \mathbf{45}_H$ model, we have identified a family of non-admissible breaking patterns towards subgroups of $SO(8) \times U(1)$ (one of the maximal subalgebras of $SO(10)$). Similar to the SM case, this family of non-admissible breakings can be parametrised by a general vacuum structure for the scalar fields $\mathbf{45}_H$ and $\mathbf{16}_H$, namely:

$$\phi_{ij} = \text{Antidiag} \left(-\omega_8, \omega_4, \omega_4, \omega_4, \omega_4, -\omega_4, -\omega_4, -\omega_4, -\omega_4, \omega_8 \right), \quad (4.9)$$

and

$$\chi = \frac{1}{\sqrt{2}} \left(i\chi_4, -i\chi_5, 0, 0, 0, 0, i\chi_4, i\chi_5, -\chi_4, \chi_5, 0, 0, 0, 0, \chi_4, \chi_5 \right)^T. \quad (4.10)$$

We stress that the vev χ_5 that appears in the above expression has the same origin that in the vev texture (4.6) for the SM breakings. The choice of gauge that we have made in the

above parameterisation makes it manifest. With these vev textures, the vacuum manifold takes the general form

$$\begin{aligned} \langle V \rangle = & \lambda_1 (\omega_8^2 + 4\omega_4^2)^2 + \frac{\lambda_2}{4} (\omega_8^4 + 24\omega_8^2\omega_4^2 + 40\omega_4^4) + 4\lambda_6 (|\chi_4|^2 + |\chi_5|^2)^2 + 8\lambda_7 |\chi_4|^2 |\chi_5|^2 \\ & + 4\lambda_8 (|\chi_4|^2 + |\chi_5|^2) (\omega_8^2 + 4\omega_4^2) + \lambda_9 \left(|\chi_4|^2 (\omega_8 - 4\omega_4)^2 + |\chi_5|^2 (\omega_8 + 4\omega_4)^2 \right), \end{aligned} \quad (4.11)$$

and its similarity with the SM vacuum manifold is worth noticing. When $\omega_4, \omega_8 \neq 0$ and either $\chi_4 \neq 0$ or $\chi_5 \neq 0$, this vacuum manifold corresponds to a breaking towards $SU(4) \times U(1)$. Imposing particular relations on the vevs yields larger residual gauge groups such as $SO(8) \times U(1)$, $SO(7)$ and $SU(4) \times U(1)^2$, as reported in Table 1.

Finally, we note that an additional vev texture for $\mathbf{45}_H$ was considered in this work, leading to an alternative embedding of $SU(4) \times U(1)^2$ within $SO(8) \times U(1)$ (stemming from the so-called triality property of $SO(8)$). This additional embedding only involves a non trivial vev texture for $\mathbf{45}_H$, given by

$$\phi_{ij} = \text{Antidiag} \left(\omega_8, \omega'_4, 0, 0, 0, 0, 0, 0, -\omega'_4, -\omega_8 \right). \quad (4.12)$$

It is interesting to note that the constraint $\omega'_4 = \omega_8$ induces a breaking towards $4_C 2_L 1_R$, of which $SU(4) \times U(1)^2$ is indeed a subgroup. As discussed in the next section, this alternative breaking actually never occurs for group-theoretical reasons.

4.2.3 Non-observable broken phases

In a gauge theory with a specified particle content, a limited number of gauge invariants can be formed. Allowing these invariants to get non-zero expectation values defines gauge-orbits in the field space. Each gauge orbit is associated with a residual symmetry group (the orbit's little group), and the set of gauge orbits associated with the same residual symmetry forms a stratum [44]. Specifying the scalar potential of the theory fixes the stratum structure, and therefore the number of subgroups that can be obtained after spontaneous breakdown of the original symmetry. Those strata (and associated phases) will be called observable if there exists a field configuration minimising the scalar potential and leading to the spontaneous breakdown of the gauge group towards the associated subgroup [45, 46]. In the model considered in this work, some strata (or equivalently some broken phases) can be shown to be non-observable at tree level. This is in particular the case of the $3_C 2_L 1_R 1_{B-L}$, $SU(4) \times U(1)^2$ and $[SU(4) \times U(1)^2]'$ strata. For concreteness, we now provide a proof of this statement for the $3_C 2_L 1_R 1_{B-L}$ breaking. Let us first consider that the scalar potential includes scalar mass couplings, and in particular the following operator:

$$V^{(0)} \supset -\frac{1}{4} \mu_\phi \text{Tr}(\Phi_{16}^2). \quad (4.13)$$

In this case, the $3_C 2_L 1_R 1_{B-L}$ vacuum manifold reads:

$$V^{(0)} = -\mu_\phi (3\omega_B^2 + 2\omega_R^2) + \lambda_1 (3\omega_B^2 + 2\omega_R^2)^2 + \frac{\lambda_2}{4} (21\omega_B^4 + 36\omega_B^2\omega_R^2 + 8\omega_R^4). \quad (4.14)$$

Solving the stationary point equations with respect to $\omega_{B,R}$ yields the set of solutions (excluding the trivial solution $\omega_B = \omega_R = 0$)

$$(\omega_B^2, \omega_R^2) \in \left\{ \left(0, \frac{\mu_\phi}{4\lambda_1 + 2\lambda_2} \right), \left(\frac{2\mu_\phi}{12\lambda_1 + 7\lambda_2}, 0 \right), \left(\frac{2\mu_\phi}{20\lambda_1 + 13\lambda_2}, \frac{2\mu_\phi}{20\lambda_1 + 13\lambda_2} \right) \right\}. \quad (4.15)$$

These three solutions respectively belong to gauge orbits associated with the residual subgroups $4_C 2_L 1_R$, $3_C 2_L 2_R 1_{B-L}$ and $SU(5) \times U(1)$, and we conclude that the $3_C 2_L 1_R 1_{B-L}$ broken phase is non-observable. This statement persists in the classically scale-invariant regime considered in this work (*i.e.* in absence of scalar mass terms), when one examines the residual gauge group along the flat directions of the vacuum manifold. A similar reasoning applies to the $SO(10) \rightarrow [SU(4) \times U(1)^2]'$ vacuum manifold which effectively corresponds to a $SO(10) \rightarrow SU(5) \times U(1)$ breaking after minimisation.

At this point, we would like to make an important comment regarding the $3_C 2_L 2_R 1_{B-L}$ and $4_C 2_L 1_R 1_{B-L}$ breakings studied in *e.g.* [5, 21, 22, 47]. In particular, still in presence of a scalar mass term in the tree-level potential, it is straightforward to compute the depth of the minimum in the following vacuum configurations:

$$V_{3_C 2_L 2_R 1_{B-L}}^{\min} = \frac{-3\mu_\phi^2}{12\lambda_1 + 7\lambda_2}, \quad (4.16)$$

$$V_{4_C 2_L 1_R 1_{B-L}}^{\min} = \frac{-\mu_\phi^2}{4\lambda_1 + 2\lambda_2}, \quad (4.17)$$

$$V_{SU(5) \times U(1)}^{\min} = \frac{-5\mu_\phi^2}{20\lambda_1 + 13\lambda_2}. \quad (4.18)$$

We can add to this list the depth of the minimum in a $SO(8) \times U(1)$ vacuum configuration:

$$V_{SO(8) \times U(1)}^{\min} = \frac{-\mu_\phi^2}{4\lambda_1 + \lambda_2}. \quad (4.19)$$

With these expressions at hand, we may establish a hierarchy for the depth of the minima in these four vacuum configurations⁸, see also [48]:

$$V_{SO(8) \times U(1)}^{\min} < V_{4_C 2_L 1_R 1_{B-L}}^{\min} < V_{3_C 2_L 2_R 1_{B-L}}^{\min} < V_{SU(5) \times U(1)}^{\min} \quad \text{if } \frac{\lambda_2}{\lambda_1} > 0, \quad (4.20)$$

$$V_{SO(8) \times U(1)}^{\min} > V_{4_C 2_L 1_R 1_{B-L}}^{\min} > V_{3_C 2_L 2_R 1_{B-L}}^{\min} > V_{SU(5) \times U(1)}^{\min} \quad \text{if } \frac{\lambda_2}{\lambda_1} < 0, \quad (4.21)$$

$$V_{SO(8) \times U(1)}^{\min} = V_{4_C 2_L 1_R 1_{B-L}}^{\min} = V_{3_C 2_L 2_R 1_{B-L}}^{\min} = V_{SU(5) \times U(1)}^{\min} \quad \text{if } \lambda_2 = 0. \quad (4.22)$$

From the above inequalities, a critical observation is that the $3_C 2_L 2_R 1_{B-L}$ and $4_C 2_L 1_R 1_{B-L}$ vacua cannot correspond to global minima, except perhaps in the limiting case where $\lambda_2 = 0$, in which loop corrections to the scalar potential would have to be included to remove the

⁸Note that when $\lambda_1 = 0$, the conditions $\frac{\lambda_2}{\lambda_1} > 0$ and $\frac{\lambda_2}{\lambda_1} < 0$ must be respectively replaced by $\lambda_2 > 0$ and $\lambda_2 < 0$.

degeneracy. Such phases are referred to as *locally* observable in Table 1, reflecting their property to only corresponding to local minima at tree-level, or to belonging at best to a degenerate set of global minima in a rather fine-tuned setting.

Table 1: Summary of the considered breaking patterns. In each case, we indicate which vevs should be non-zero in order to trigger spontaneous breakdown towards the relevant subgroups. A starred vev (*e.g.* ω_8^*) can however vanish without altering the nature of the vacuum. As explained in the main text, non-observable phases correspond to minima which cannot be global, while non-admissible breakings occur towards subgroups of $SO(10)$ which do not contain the Standard Model. An admissible breaking is called viable if it can obey the proton stability and gauge coupling unification constraints (more detail is given in Sec. 4.2.4).

Breaking chain	Vevs	Observable?	Admissible?	Viable?
$SU(5) \times U(1)$	$\omega_R = \omega_B$	Yes	Yes	Yes
$SU(5)$	$\omega_R^* = \omega_B^*, \chi_5$	Yes	Yes	No
$3_C 2_L 2_R 1_{B-L}$	ω_B, χ_5	Yes, locally	Yes	Yes
$4_C 2_L 1_R$	ω_R, χ_5	Yes, locally	Yes	Yes
$3_C 2_L 1_R 1_{B-L}$	ω_R, ω_B	No	Yes	Yes
$3_C 2_L 1_Y$	$\omega_R, \omega_B, \chi_5$ or χ_R	Yes	Yes	Yes
$SO(8) \times U(1)$	ω_8	Yes	No	No
$SO(7)$	$\omega_8^*, \chi_4 = \chi_5$	Yes	No	No
$SU(4) \times U(1)^2$	ω_8^*, ω_4	Yes	No	No
$[SU(4) \times U(1)^2]'$	ω_8^*, ω_4'	No	No	No
$SU(4) \times U(1)$	$\omega_8, \omega_4, \chi_4$ or χ_5	Yes	No	No

4.2.4 Viability of admissible breaking patterns

We conclude this section by a discussion on the viability of the breaking chains eventually leading to the Standard Model. These admissible breakings are summarised in Table 1. Independently of the observable property of the $SO(10)$ vacua (which is *a priori* dependent of the perturbative order of the quantum scalar potential), a viable breaking is understood to feature desirable (and non-excluded) phenomenological properties in the low-energy regime (*e.g.* down to the electroweak scale). In its strongest version, such a definition encompasses a large number of criteria such as proper gauge coupling unification, a proton decay constant large enough to evade current experimental bounds, a fermion and scalar spectrum containing the Standard Model and compatible with negative new physics searches, among many others. In this work, we will solely retain the first two criteria since any further considerations are beyond the scope of the present analysis⁹.

⁹Furthermore, as mentioned in Sec. 4.1, the $SO(10)$ model investigated here is anyways unable to reproduce some phenomenological features of the Standard Model.

First focusing on the Georgi-Glashow route, the one-step unification $SU(5) \rightarrow 3_C 2_L 1_Y$ is not supported by the current measurements of the Standard Model gauge couplings, thus bringing us to regard the $SU(5)$ breaking as non-viable. On the other hand, the $SU(5) \times U(1) \rightarrow 3_C 2_L 1_Y$ embedding (flipped or standard, see Sec. 4.2.1) can be realised if large thresholds¹⁰ are present [19], thus implying large hierarchies in the scalar and gauge boson spectrum at the $SO(10)$ -breaking scale. Combined with constraints stemming from the proton decay, this scenario is rather tightly constrained yet not ruled out.

For the Pati-Salam route including the breakdown of $SO(10)$ towards $4_C 2_L 1_R$, $3_C 2_L 2_R 1_{B-L}$ and $3_C 2_L 1_R 1_{B-L}$, we refer to [22] and conclude that gauge coupling unification and proton-decay constraints can be satisfied for the first two breakings. On the other hand, $SO(10) \rightarrow 3_C 2_L 1_R 1_{B-L}$ is shown in [19] to require sizeable threshold corrections in order to allow for a proper unification of the gauge-couplings. This being said, we have mentioned in the introduction of this section that the $4_C 2_L 1_R$, $3_C 2_L 2_R 1_{B-L}$ and $3_C 2_L 1_R 1_{B-L}$ breakings have long been disregarded due to the presence of tachyonic scalar modes in their tree-level spectrum (put differently, the corresponding extrema can only be saddle points [40–42, 50]). More recently, it has been shown that the inclusion of one-loop corrections could stabilise the scalar potential [5, 21, 47], rendering such breaking patterns potentially viable. What the authors did not consider however is the eventuality that a deeper minimum triggering a breakdown towards $SO(8) \times U(1)$ would prevent the Pati-Salam vacua to correspond to global minima. While this statement was proven at tree-level in the previous section, one cannot infer *a priori* that the non-observability of the Pati-Salam vacua would persist after including loop-corrections. In Sec. 5, we investigate this matter and show that in fact, the inclusion of one-loop corrections does not change this overall picture (at least in the particular model considered here).

Finally, we comment on the viability of the one-step $SO(10) \rightarrow 3_C 2_L 1_Y$ breaking. As compared to the $SU(5) \rightarrow 3_C 2_L 1_Y$ embedding mentioned above, gauge coupling unification does not necessarily have to occur at once (i.e. at a single unification scale). In fact, an effective description of the model from the UV to the IR regime can include multiple intermediate scales at which massive gauge bosons are integrated out, and between which different sets of gauge couplings are assumed to run. This happens in particular if a clear hierarchy appears between the various vevs involved in the description of the vacuum manifold after minimisation of the scalar potential (see also the discussion on standard and flipped $SU(5) \times U(1)$ embeddings in Sec. 4.2.1). Such a situation most likely involves rather fine-tuned relations among the parameters of the scalar potential, which we however do not consider as a criterion for the non-viability of the model.

¹⁰Let us note that these corrections can be straightforwardly calculated within our approach and are indeed subject to the investigation in the following paper [49]. here we simply assume that such a scenario can take place.

5 Results

With the RG-improved effective potential formalism, cf. Sec. 3, and the group-theoretical structure of the specified SO(10) GUTs, cf. Sec. 4.2 at hand, we are able to demonstrate how the EFT parameter space of said GUTs is restricted by the various constraints on a viable scalar potential, cf. Sec. 2. In order to determine these constraints, we sample random initial conditions to map out how each constraint reduces the potentially available parameter space. We do so first for a model with $\mathbf{45}_H$ as the only scalar representation, cf. Sec. 5.1. We then extend the analysis to a model with $\mathbf{45}_H$ and $\mathbf{16}_H$ scalar representations, cf. Sec. 5.2. An extension of our analysis to a model with realistic Yukawa sector will be discussed in future work [].

The scalar potential is not only driven by self-interactions but more importantly also by contributions from the gauge coupling g_{10} and potential Yukawa couplings. The gauge coupling g_{10} tends to destabilise the quartic scalar potential, i.e., tends to induce radiative symmetry breaking [11]. Hence, the RG-flow-dependent value of g_{10} is a crucial input to explicitly determine constraints on the scalar potential. At the same time, g_{10} itself also needs to be matched to the observed low-energy gauge-coupling values. To maintain this matching, its viable initial value at M_{Pl} thus needs to be varied with any variations of the RG-flow of g_{10} between M_{Pl} and M_{EW} . The respective uncertainties include higher-loop corrections but are dominated by the dependence on different breaking schemes and breaking scales [5, 22]. In principle, one may thus also sample over different values of $g_{10}|_{M_{\text{Pl}}}$, in particular using the one-loop RGEs $g_{10}|_{M_{\text{Pl}}} \in (0.4, 0.45)$. Since we only aim to demonstrate the restrictive power of the applied constraints arising in the scalar potential, we do not do so in the following. Rather, we pick a fixed value

$$g_{10}|_{M_{\text{Pl}}} = 0.435 . \tag{5.1}$$

In principle, all of the above also holds for Yukawa couplings. Based on [11], we expect Yukawa couplings to have a stabilising effect on the quartic couplings of representations to which they can couple [?]. Most excitingly, this provides a potential mechanism for a hierarchy of several breaking scales. However, neither of the presently investigated scalar potential admits Yukawa couplings to the fermionic $\mathbf{16}_F$, i.e., to SM fermions.

In order to demonstrate the restrictive power of each constraint, cf. Sec. 2, we will apply the constraints individually: First, we demand tree-level stability (I.a); second, we demand perturbativity between M_{Pl} and M_{GUT} (I.b); third, we demand that the deepest vacuum be an admissible one (I.c), i.e., one which still remains invariant under the SM gauge group \mathcal{G}_{SM} . Since the last constraint is conceptually new, we emphasise two important points.

The first concerns the inclusion of non-admissible breaking chains. On the one hand, a successful application requires the inclusion of all admissible vacua in order to make sure that ruled out EFT parameter space may in fact not be admissible. On the other hand, it does not require the inclusion of all nonadmissible vacua. The more nonadmissible vacua

are included, the more one restricts the EFT parameter space, cf. Sec. 4.2 for the respective group-theoretical discussion for the cases at hand.

The second concerns the possible spontaneous symmetry breaking by additional mass terms, which we neglect in the present study. Indeed, the admissibility-constraints remain partially applicable also in the presence of mass terms. This is because while mass terms can induce additional breaking scales $M_{\text{GUT-mass}}$, the investigated radiative symmetry breaking scales M_{GUT} will presumably remain present. In order for a mass term to change conclusions about an otherwise excluded region of EFT parameter space, the mass-induced symmetry-breaking scale $M_{\text{GUT-mass}}$ (breaking to an admissible subgroup) must thus be larger than the radiatively induced breaking scale M_{GUT} (breaking to a nonadmissible subgroup). In addition to these sets of constraints (I.a-I.c) arising from an admissible scalar potential, one may also apply more commonly discussed constraints arising from (II.a) viable gauge unification and (II.b) a viable Yukawa sector. As mentioned, (II.b) does not apply to the investigated models. The application of the gauge-unification constraint (II.a), to the remaining admissible parameter space after application of (I.a-I.c), is briefly discussed in case of the $\mathbf{45}_H$, cf. Sec. 5.1.

5.1 Constraints from an $\text{SO}(10)$ model with $\mathbf{45}_H$ scalar potential

An $\text{SO}(10)$ GUT with the $\mathbf{45}_H$ as the only scalar representation cannot fully break to the SM. Nevertheless, the $\mathbf{45}_H$ is responsible for the first breaking step in many realistic $\text{SO}(10)$ -breaking chains, cf. Tab. 1. It thus serves as a simplified toy model for the first breaking step. The simplification is justified whenever portal couplings to other scalar representations remain negligibly small. Note that it is not consistent to simply set the portal couplings to zero since they are not protected by any global symmetry and thus induced by loop corrections. The $\mathbf{45}_H$ -model is thus a good approximation for a realistic first breaking step only in a regime in which portal couplings remain negligibly small. The subsequent extension to a scalar potential with $\mathbf{45}_H$ and $\mathbf{16}_H$ representation, cf. Sec. 5.2, can be interpreted as a test of this approximation. Indeed, we will see that the main constraint on the EFT parameter space – while washed out – will still remain important if the scalar potential is extended.

Group-theoretically, the $\mathbf{45}_H$ can break $\text{SO}(10)$ to three different classes of observable vacua, cf. Tab. 1 and Sec. 4 for details:

- Admissible Georgi-Glashow direction: The $\mathbf{45}_H$ can break towards $SU(5) \times U(1)$ which still contains the SM.
- Admissible Pati-Salam directions: The $\mathbf{45}_H$ can break towards two different Pati-Salam-type directions, i.e., to $3_C 2_L 2_R 1_{B-L}$ or $4_C 2_L 1_R$, which also still contain the SM.
- Non-admissible directions: The $\mathbf{45}_H$ can also break $\text{SO}(10)$ towards two non-admissible directions, i.e., to $SO(8) \times U(1)$ or $SU(4) \times U(1)^2$, which can no longer contain the SM and are therefore excluded.

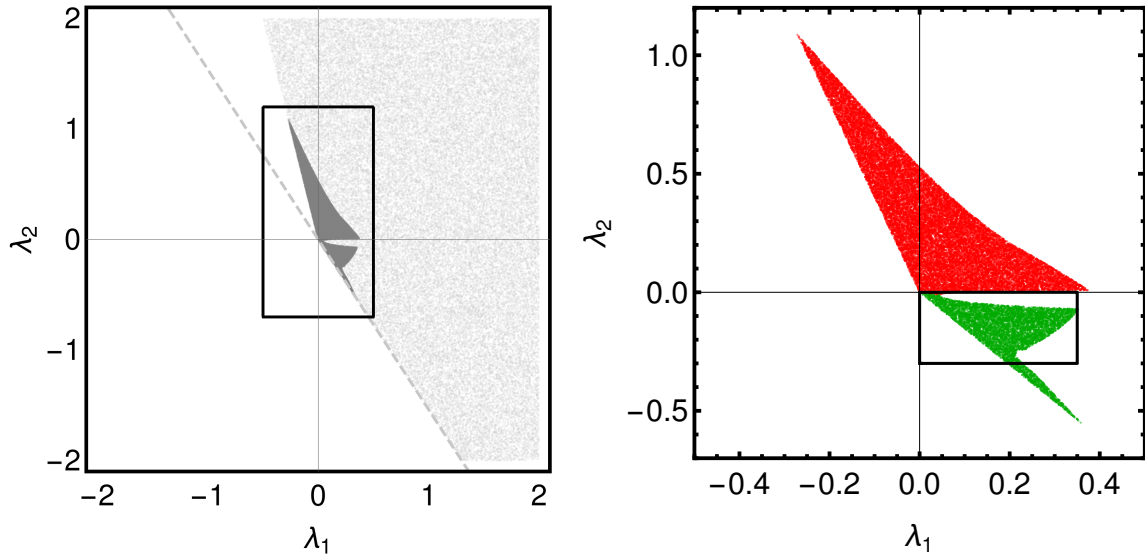


Figure 1: Successive constraints arising from an admissible scalar potential, cf. Sec. 2, on the Planck-scale theory space of quartic couplings in an $SO(10)$ GUT with $\mathbf{45}$ scalar matter content. The left-hand panel shows constraints arising from (I.a) stability (light-gray region) and from (I.b) perturbativity (dark-gray region). The right-hand panel zooms in on the resulting stable and perturbative region and shows additional constraints (I.c) arising from the deepest radiative minimum occurring in a nonadmissible direction (red region). The green region in the right-hand panel remains potentially viable. It is further constrained by a viable gauge (and more generally gauge-Yukawa) sector, cf. Fig. ??.

One of the important results of this work is that we find that the Pati-Salam directions can never occur as global minima: Either the Georgi-Glashow minima or the non-admissible minima are always deeper. This statement is proven at tree-level in Sec. 4.2.3. We find that it persists when radiative effects are included. In fact, we find that all initial conditions either break towards $SU(5) \times U(1)$ or towards $SO(8) \times U(1)$.

The $\mathbf{45}_H$ toymodel also demonstrates clearly how the three scalar-potential constraints, i.e., tree-level stability (I.a), perturbativity (I.b), and admissibility (I.c), successively constrain the EFT parameter space at M_{Pl} . This is presented in Fig. 1, where we summarise the results of a successive analysis of uniformly distributed random initial conditions for λ_1 and λ_2 .

First, we determine tree-level stability: Stable initial conditions are marked with light-gray points in the left-hand panel of Fig. 1. The dashed line corresponds to the analytical condition for tree-level stability, cf. Eq. (3.23). Clearly, the analytical condition is necessary but not sufficient.

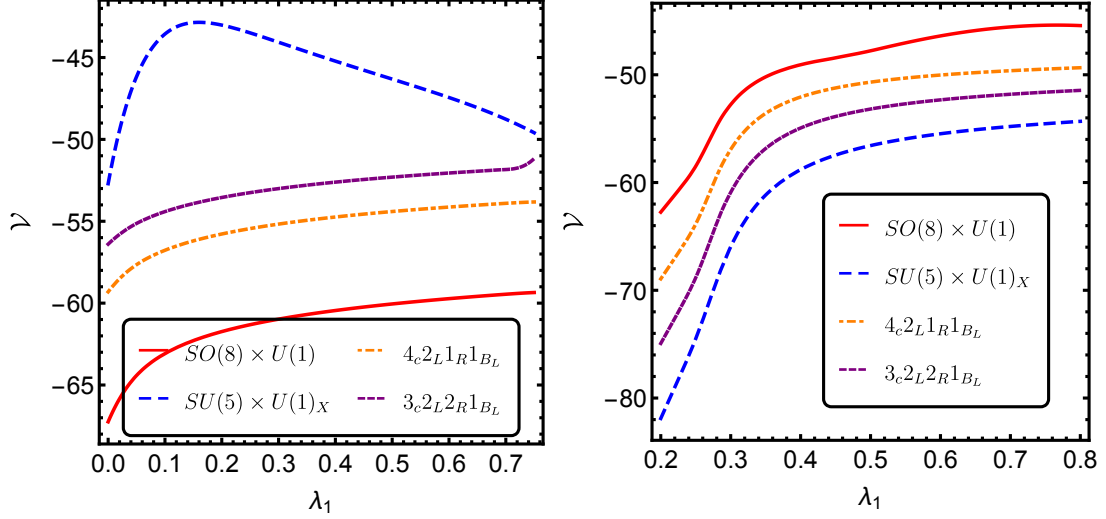
Second, we apply the perturbativity constraint: Initial conditions which remain sufficiently perturbative along the relevant RG-flow towards lower scales are marked with

dark-gray points in the left-hand panel of Fig. 1. Unfortunately, we are not aware of a strict perturbativity criterion. The detailed perturbativity criterion, extending a proposed criterion in [51], is discussed in App. C. It amounts to the demand that the theory-space norm of neglected 2-loop contributions does not outgrow a specified fraction α of the theory-space norm of 1-loop contributions. For all the results in this work, we pick $\alpha = 0.1$ which might be overly conservative but allows us to avoid convergence issues in the subsequent numerical determination of the 1-loop effective potential and its deepest minimum. In practice, perturbativity is determined as follows: We pick a random point in the interval $\lambda_{1/2} \in [-2, 2]$. (If the point violates tree-level stability, we pick again.) We evolve the respective initial conditions towards lower scales until the analytical conditions in Sec. ?? suggest that radiative symmetry breaking occurs. If the RG-flow remains perturbative until radiative symmetry breaking occurs, the respective initial conditions pass the perturbativity criterion (dark-gray region in the left-hand panel of Fig. 1). We iterate this procedure for 10^7 points.

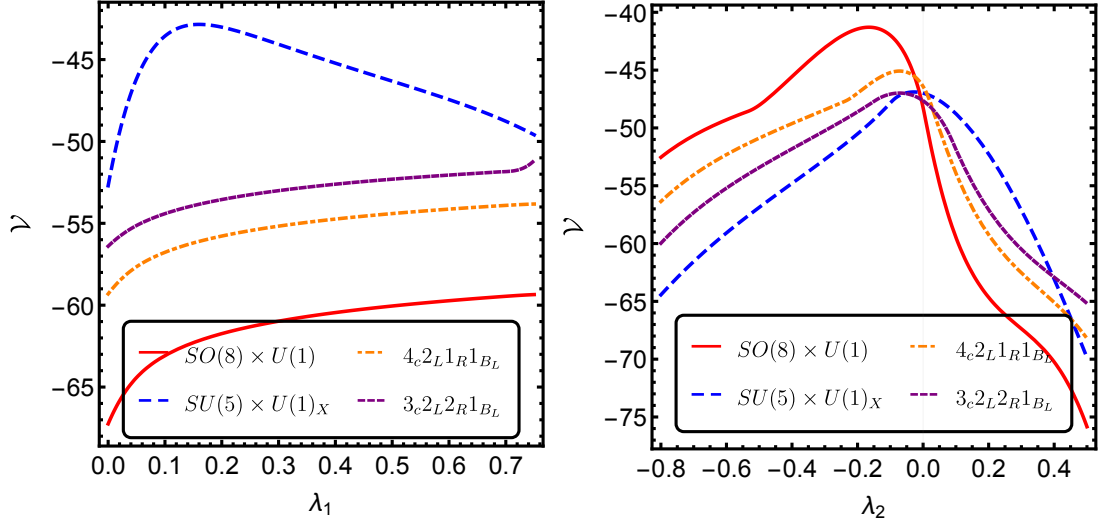
Third, we apply the admissibility criterion: For initial conditions which pass tree-level stability and perturbativity, we determine the 1-loop effective potential, the deepest minimum, and the respective invariant subgroup (breaking direction). Construction of the 1-loop effective potential following [] and the numerical method are detailed in Sec. 3. Keeping with tree-level expectations in Sec. 4.2.3, we find that the global minimum occurs either in the admissible $SU(5) \times U(1)$ direction (green region in the right-hand panel in Fig. 1) or in the nonadmissible $SO(8) \times U(1)$ direction (red region in the right-hand panel in Fig. 1). To explicitly demonstrate that we include the exemplary plots of the potential minima in different directions. Observe, that when $SO(8) \times U(1)$ vacuum is not included, then indeed Pati-Salam vacua can be the deepest minima for some regions in the parameter space, as reported in [5, 47, 52]. However after the inclusion of the $SO(8) \times U(1)$ vacua the Pati-Salam are never the deepest vacua. Furthermore one can observe on Figures 2c, 2d that there is a strong degeneracy of the vacua at $\lambda_2 \approx 0$. This degeneracy comes from the fact that all of the vacua have the same stability condition at that point namely $\lambda_1 > 0$ and that starting from $\lambda_2(\text{M}_{\text{Pl}})$ results $\lambda_2(\mu) \approx 0$ along the flow. Such a degeneracy is however dangerous to the predictivity of the model, not only it implies different low-energy theories throughout the space, but also gives rise to the long-living domain-walls dominating the Universe [53–56] and hence is forbidden phenomenologically.

In summary: First, the Planck-scale theory space of quartic couplings is significantly constrained by demanding an admissible scalar potential. Second, the 1-loop effective potential will never develop a deepest minimum along a Pati-Salam-type breaking direction.

We proceed to test how robust these conclusions are, when including both a $\mathbf{16}_H$ along with the $\mathbf{45}_H$ scalar representation.



(a) The dependence of depth of minima on λ_1 for $\lambda_2 = 0.1$. (b) The dependence of depth of minima on λ_1 for $\lambda_2 = -0.4$.



(c) The dependence of depth of minima on λ_2 for $\lambda_1 = 0.1$. (d) The dependence of depth of minima on λ_2 for $\lambda_1 = 0.7$.

Figure 2: The \mathcal{V} denotes the minus log of the depth of the vacuum expectation value. Given $\lambda_1|_{\text{M}_{\text{Pl}}}, \lambda_2|_{\text{M}_{\text{Pl}}}$ we present the relative depth of the minimas in the logarithmic scale.

5.2 Constraints from an $\text{SO}(10)$ model with $16_H \oplus 45_H$ scalar potential

Including the 16_H and 45_H scalar representation, the quartic scalar potential is 6-dimensional, cf. App. (??). This entails additional breaking chains which are discussed in detail in Sec. 4.2 and summarised in Tab. 1.

We obtain a sample of 10^5 random points in the region $\lambda_i \in [-1, 1]$ and proceed as in Sec. 5.1 by successively applying the three constraints on the scalar potential, cf. Sec. 2. For each successive constraint, we only take into account points which have passed the

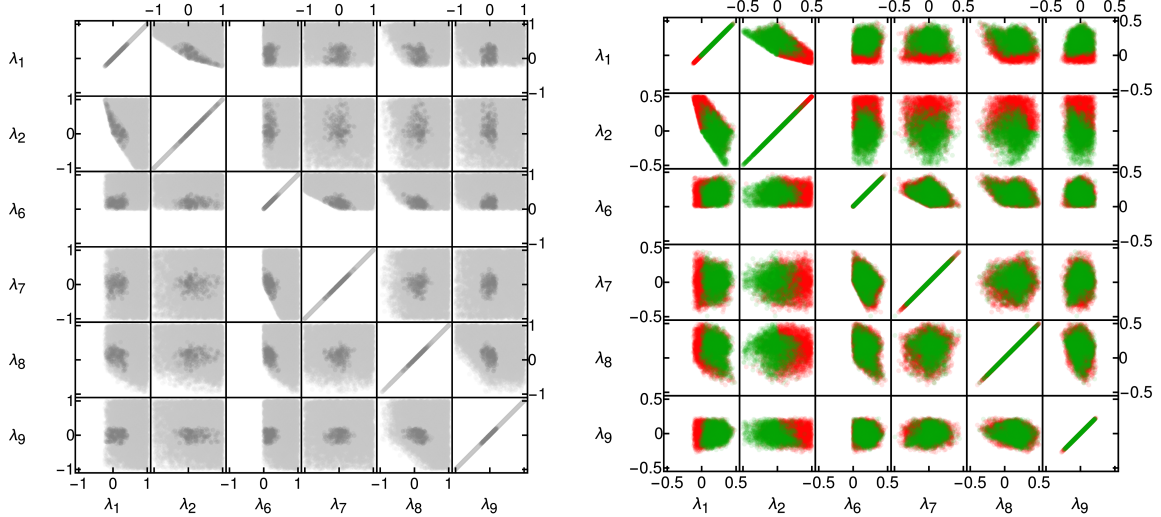


Figure 3: Successive constraints (I.a-c), cf. Sec. 2, on the 6-parameter Planck-scale theory space of quartic couplings in an $\text{SO}(10)$ GUT with $\mathbf{16} + \mathbf{45}$ scalar matter content. The left-hand panel shows a statistical scatter-plot matrix of constraints arising from (I.a) stability (light-gray regions) and from (I.b) perturbativity (dark-gray regions). The right-hand panel shows a zoomed-in scatter-plot matrix of additional constraints (I.c) arising from the deepest radiative minimum occurring in a nonadmissible direction (red regions). The green regions in the right-hand panel remain potentially viable.

previous constraints. The results are shown in Fig. 3. We present them in the form of statistical scatter-plot matrices which project the 6D parameter space onto a full set of 2D slices. While this can reveal important correlation, it also leads to a perceived blurring of presumably sharp boundaries in the full higher-dimensional parameter space.

First, we determine tree-level stability: Stable initial conditions are marked with light-gray points in the left-hand panel of Fig. 3. The stability-constraints on the pure- $\mathbf{45}_H$ -couplings λ_1 and λ_2 remain the same as for the case without $\mathbf{16}_H$. There is a similar constraints on the pure- $\mathbf{16}_H$ -couplings λ_6 and λ_7 . Finally, also the portal couplings λ_8 and λ_9 are constrained by demanding tree-level stability of the initial conditions.

Second, we apply the perturbativity constraint: Initial conditions which also remain perturbative between M_{Pl} and M_{GUT} , are marked in the left-hand panel of Fig. 3 as dark-gray points. We remind the reader that we determine perturbativity by demanding that the theory-space norm of neglected 2-loop contributions does not outgrow a fraction $\alpha = 1/10$ of the theory-space norm of 1-loop contributions, cf. App. ?? for details. In keeping with an intuitive notion of perturbativity, the remaining points cluster around $\lambda_i = 0$.

Third, we apply the admissibility criterion: We obtain the 1-loop effective potential, the deepest minimum, and the respective invariant subgroup (breaking direction) to determine whether the latter is admissible, i.e., remains invariant under the SM subgroup. The results

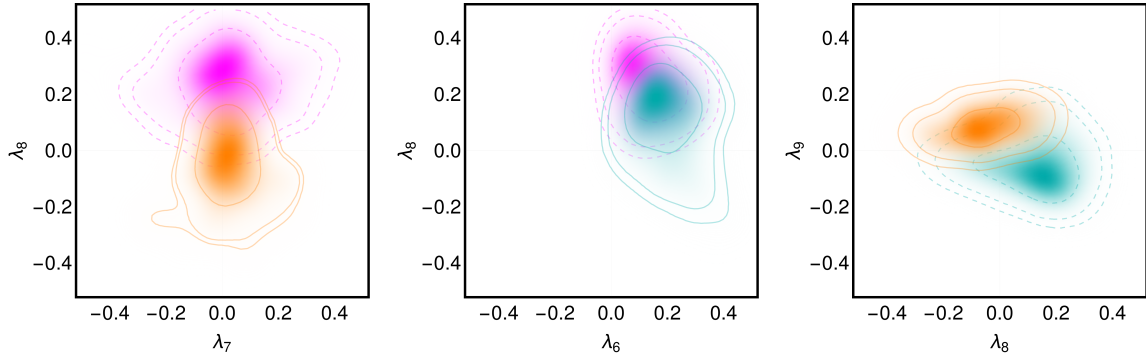


Figure 4: Probability-density functions (PDFs) of pairs of different admissible breakings ($SU(5)$ in cyan; $SU(5) \times U(1)$ in magenta; $SU(3) \times SU(2) \times U(1)$ in orange) for selected projections into 2-dimensional slices of theory space. Contour lines indicate the 1σ -, 2σ -, and 3σ -regions obtained with a Gaussian kernel of width 0.05. We only show those projections which best discriminate the two respective breaking patterns. The full scatter-plot matrices are given in App. ??.

are presented in the right-hand panel of Fig. 3 where due to significant constraints from perturbativity, we focus only on the remaining subregion $\lambda_i \in [-0.5, 0.5]$. (Non-) Admissible points are shown in green (red). We find that the pure- $\mathbf{45}_H$ couplings λ_1 and λ_2 are still dominant in determining whether stable and perturbative initial conditions are also admissible or not. At the same time, non-vanishing portal couplings can apparently alter admissibility-constraints on pure- $\mathbf{45}_H$ couplings λ_1 and λ_2 , cf. right-hand panels of Fig. 1 and Fig. 3. In particular, the admissible region in a λ_1 - λ_2 projection of theory space grows when the $\mathbf{16}_H$ is included: This occurs because there are additional admissible breaking patterns in comparison to the pure- $\mathbf{45}_H$ case, cf. Tab. 1. This includes an admissible $SU(5)$ breaking and, in principle, an admissible direct breaking to the SM, i.e., to $SU(3) \times SU(2) \times U(1)$. In particular, the $SU(5)$ -breaking can occur as the deepest vacuum, even for $\lambda_2 > 0$. This adds admissible initial conditions with λ_1 - λ_2 which were previously excluded in the pure- $\mathbf{45}_H$ model.

Whether and if so which of these admissible vacua is the deepest one depends on the initial conditions of all of the six quartic couplings. Fig. 4 shows the most prominent correlations that we were able to identify. We emphasise that there are still no initial conditions with admissible Pati-Salam type breaking.

In summary: The main constraints from stability and perturbativity are robust under the extension of the $\mathbf{45}_H$ to the $\mathbf{16}_H \oplus \mathbf{45}_H$ scalar potential. While Pati-Salam type breakings remain non-admissible, other admissible breakings can occur.

6 Discussion

We end this paper with (i) a brief summary of the results of the present work, (ii) some comments on trans-Planckian extensions in existing quantum-gravity scenarios, and (iii) an outlook on what we consider the most important open questions.

6.1 Summary of the main results

We have initiated a systematic study of how radiative symmetry breaking to non-admissible vacua places significant constraints on the initial conditions of any potentially viable grand-unified effective field theory (GUEFT). We embed this novel constraint in a systematic set of constraints, some of which have been previously discussed in the literature. The resulting blueprint is given in Sec. 2. It encompasses several constraints on the scalar sector: (I.a) a tree-level stability constraint, (I.b) a perturbativity constraint on quartic couplings, and (I.c) the above-mentioned novel requirement of admissible vacua. These scalar-potential constraints supplement well-known requirements on a viable gauge-Yukawa sector, cf. Sec. 2 as well as [1].

As a first application, we exemplify these constraints in an $SO(10)$ GUT with three families of $\mathbf{16}_F$ fermionic representations and a scalar potential build from a $\mathbf{16}_H$ and a $\mathbf{45}_H$ representation. Therein, we have demonstrated how each successive application of the constraints (I.a), (I.b), and (I.c) reduces the admissible parameter space of initial conditions.

The above concrete model yet lacks a sufficiently large Yukawa sector to account for the Standard-Model Yukawa sector. Still, we were able to draw some important specific conclusions. Firstly, we find that previously neglected non-admissible breaking directions prohibit any possibility of radiative symmetry breaking to the Standard Model via Pati-Salam type intermediate vacua. This conclusion exemplifies that (I.c) poses a novel but highly significant constraint on GUEFTs.

6.2 Comments on a link to three specific quantum-gravity scenarios

Our main motivation to systematically constrain the viable Planck-scale parameter space of GUEFTs is a promising connection to quantum-gravity (QG) scenarios. If such a link can be drawn, the predictive power of QG scenarios may provide a further set of constraints (III) on the Planck-scale initial conditions. Vice versa, GUEFTs provide a possible arena for experimentally accessible indirect tests of QG. This is because, as our work clearly demonstrates, viable IR phenomenology is impacted by Planck-scale initial conditions.

Before providing an outlook on future work, we thus briefly comment on three QG scenarios in which we see a promising route to make this link explicit. It is useful to distinguish between two possibilities.

On the one hand, there are QG scenarios which remain within the framework of quantum field theory. In this case, gravitational fluctuations will simply provide additional

contributions to the Renormalisation Group (RG) flow of beta functions of the GUEFT, i.e.,

$$\beta_{c_i} = \beta_{c_i}^{(\text{GUEFT})} + \beta_{c_i}^{(\text{gravity})} . \quad (6.1)$$

Herein, c_i denotes the collection of all GUEFT couplings. Typically, one then demands β_{c_i} to lead to a UV-complete theory. With sufficient insight into the gravitational contributions $\beta_{c_i}^{(\text{gravity})}$ such a UV-completion implies additional constraints on the parameter space at the Planck scale. We will comment on two such scenarios – Complete Asymptotic Freedom as well as Asymptotic Safety – below.

On the other hand, there are QG scenarios which cannot be phrased in the framework of quantum field theory. Nevertheless, in order to be consistent with observations, they have to provide a limit – typically associated with the Planck scale – in which an EFT description emerges as a low-energy limit. Hence, there again must be some way of extracting predictions about the GUEFT couplings at the Planck scale. We will briefly comment on the case of string theory below.

Complete Asymptotic Freedom

Some QG scenarios suggest that even at trans-Planckian scales, gravity decouples from the matter sector, cf. e.g. [57? ?]. In practice, such scenarios thus amount to simply extrapolating the SM or, in the present context, the respective GUEFT beyond the Planck scale, i.e.,

$$\beta_{c_i}^{(\text{gravity})} = 0 , \quad (6.2)$$

in Eq. 6.1. We note that, in any such QG scenario, the Standard Model remains UV-incomplete due to the U(1) Landau-pole. This obstruction, however, can be avoided in a GUT where the U(1) Abelian gauge group at high energies is part of a non-Abelian gauge group with self-interactions. Said self-interactions can – depending on the respective gauge group and matter content – be sufficiently antiscreening to provide for asymptotic freedom of the gauge coupling. Even asymptotically free gauge sectors can be sufficient to also render Yukawa couplings and quartic couplings asymptotically free: a proposal known as Complete Asymptotic Freedom (CAF) of gauge-Yukawa theories¹¹. The conditions to achieve CAF in gauge-Yukawa theories have been analysed in [? ? ? ?]. Certainly, the demanding CAF without gravity places additional non-trivial constraints on the viable parameter space at the Planck scale. Such a QG scenario is thus probably the most straightforward example of additional constraints from demanding a UV-completion.

Asymptotic Safety

The asymptotic-safety scenario for QG [? ?] predicts quantum scale symmetry of gravity and matter at scales k beyond the Planck scale M_{Pl} . If asymptotic safety is realised, the

¹¹More recently, it has also been found that gauge-Yukawa theories can develop interacting fixed points with UV-attractive directions and may thus, in principle, be asymptotically safe without the presence of gravitational fluctuations []. We caution that it is unclear whether commonly discussed GUTs can realise such a scenario [].

dimensionless Newton coupling $g = G k^2$ (with G the usual dimensionful Newton coupling) transitions between classical power-law scaling $g \sim k^2$ below M_{Pl} and scale symmetry, i.e., scale-independent behaviour $g = g_* = \text{const}$ above M_{Pl} . The leading-order gravitational contribution acts like an anomalous dimension and the transition can be described, cf. [], by

$$\beta_{c_i}^{(\text{gravity})} = \begin{cases} f_{c_i} c_i + \mathcal{O}(c_i^2) + \dots & k > M_{\text{Pl}} \\ 0 & k < M_{\text{Pl}} \end{cases}. \quad (6.3)$$

with f_{c_i} constant, dependent on the gravitational fixed-point values, e.g. g_* , and, in principle, calculable from first principles. As long as all GUEFT couplings c_i remain in the perturbative regime, neglecting $\mathcal{O}(c_i^2)$ is a good approximation. Dots denote further terms by non-minimal and induced higher-order couplings, cf. [] for a discussion of these.

Due to the universal nature of gravity, $f_{c_i} \equiv f_g$ is universal for all gauge couplings; $f_{c_i} \equiv f_y$ is universal for all Yukawa couplings; and $f_{c_i} \equiv f_\lambda$ is universal for all quartic couplings. Functional RG calculations provide the following picture¹²: The gravitational contribution to gauge couplings is found to be antiscreening, i.e., $f_g \geq 0$ []; The screening or antiscreening nature of the gravitational contribution to Yukawa couplings depends on the matter content of the universe []; The gravitational contribution to quartic couplings is found to be screening, i.e., $f_\lambda < 0$ [].

Clearly, the additional antiscreening contribution f_g to the RG flow of gauge couplings will (in comparison to CAF without gravity) enlarge the Planck-scale parameter space with underlying UV-complete dynamics, cf. [] and [] for applications to the Standard Model and to GUTs, respectively.

To the contrary, the screening contribution to scalar quartic couplings (and scalar potentials in general) [] is expected to provide sharp predictions for the shape of scalar potentials, cf. [] for an application to the SM Higgs potential, [] for applications to dark-matter, and [11] for a previous discussion of GUT potentials. This is most exciting in the present context of GUEFTs since it suggests that Asymptotic Safety may fully predict the scalar potentials and thus the breaking scales and breaking directions of GUEFT models [11]. The methods developed in this work provide the basis for a systematic study of these promising ideas. The biggest outstanding caveat is the question how gravitational contributions will impact the presently applied multidimensional effective-potential methods, cf. Sec. 3.

String Theory

Let us first note that supersymmetric Grand Unification is quite natural in context of string theory, see for example [12, 15, 58–60] and references therein. In particular the heterotic String theory $E_8 \times E_8$ compactified on the Calabi-Yau threefold $SU(4)$ results in

¹²In perturbative dimensional regularisation schemes, gravitational contributions to matter couplings have also been calculated [], cf. [] for recent progress on the relation between functional RG and dimensional regularization schemes and [] for an application to gravity-matter systems.

the SUSY $SO(10)$. However the low-energy supersymmetry has not been found and the non-SUSY vacua are notoriously hard to be constructed. Yet, there exists a non-tachyonic $SO(16) \times SO(16)$ string theory with no-supersymmetry, when during compactification one gets $SO(10)$ model with $\mathbf{45}_H$ potential [14]! Since in string theory all of the low energy couplings stems from the expectation values of the “radion” fields, that is the diagonal part of the metric in the compactified dimensions. In particular in the Kaluza-Klein theory, the 4D equations resembles the Einstein-Maxwell system with the electromagnetic coupling given by some function of the diagonal 5-dimension entry g_{55} [61]. Hence, given compactification of $SO(16) \times SO(16)$ to 4-dimensions, the λ_i are not free parameters, but can be calculated.

6.3 Outlook

We see the following important extensions and applications.

First and foremost, a viable Yukawa sector \square requires an extension of the specified scalar representations from $\mathbf{16}_H \oplus \mathbf{45}_H$ to $\mathbf{16}_H \oplus \mathbf{45}_H \oplus \mathbf{126}_H$. Without such an extension, any applications to specific quantum-gravity approaches may still give tentative insights but do not present the full picture.

Within such a minimal but viable grand-unified effective field theory (GUEFT), the presented blueprint will determine which regions in parameter space correspond to a viable IR phenomenology. In such a setup, it may prove important to reconsider the respective constraints arising from non-admissible breaking directions in view of mass terms, cf. Sec. ??.

With regards to applications to concrete quantum-gravity (QG) scenarios, it seems promising to study all three approaches in Sec. 6.2. QG scenarios which reduce a study of Complete Asymptotic Freedom (CAF) are directly applicable. The QG scenario of asymptotic safety requires an extension of the effective potential to include gravitational contributions.

Overall, we are convinced that this is only the first step and that there is a promising route to connect QG approaches to a restoration of predictive power in GUEFTs.

Acknowledgments

We thank A. Eichhorn, K. Kannike, L. di Luzio, L. Marzola, B. Świeżewska and C. Wetterich for valuable discussion. During parts of this project, A. Held was supported by a Royal Society International Newton Fellowship under the grant no. NIF\R1\191008. A. Held also acknowledges that the work leading to this publication was supported by the PRIME programme of the German Academic Exchange Service (DAAD) with funds from the German Federal Ministry of Education and Research (BMBF). J.H.K. was supported by the Polish National Science Centre grants 2018/29/N/ST2/01743 and 2020/36/T/ST2/00409. L. Sartore was supported in part by the IN2P3 project “Théorie – BSMGA”.

A One-loop RG-improved potential

In this appendix, we review a certain number of useful properties and relations satisfied by the one-loop RG-improved potential introduced in section 3. In particular, we analytically justify the numerical approach used in this work to efficiently estimate the depth of the RG-improved potential in every relevant vacuum configuration in sections A.2 and A.3, and numerically evaluate its accuracy in section A.4.

A.1 Stationary point equation

In order to derive the station point equation for the RG-improved potential, it is first useful to note that the field derivatives of any RG-improved quantity $V(\phi^i, \mu_*(\phi^i))$ can be decomposed in the following way:

$$\nabla_i V(\phi, \mu_*(\phi)) = \frac{dV}{d\phi^i}(\phi, \mu_*(\phi)) = \frac{\partial V}{\partial \phi^i}(\phi, \mu_*(\phi)) + \nabla_i t_* \frac{dV}{dt}(\phi, \mu_*(\phi)). \quad (\text{A.1})$$

Namely, the total derivative with respect to the field component ϕ^i splits into a partial derivative, and a contribution stemming from the implicit dependence of the RG-scale $t_* = \log \mu_*^2$ on the field values. Next, we can readily express the stationary point equations satisfied by the RG-improved potential at an extremum:

$$\begin{aligned} \nabla_i V^{\text{eff}}(\phi, \mu_*(\phi^i)) &= \frac{\partial V^{\text{eff}}}{\partial \phi^i}(\phi, \mu_*(\phi)) + \nabla_i t_* \frac{dV^{\text{eff}}}{dt}(\phi, \mu_*(\phi)) \\ &= \partial_i V^{\text{eff}}(\phi, \mu_*(\phi)) + 2\mathbb{B}(\phi, \mu_*(\phi)) \nabla_i t_*(\phi) = 0, \end{aligned} \quad (\text{A.2})$$

where we used in the last step the first order truncated Callan-Symanzik equation (3.7) (see *e.g.* [18]):

$$\frac{dV^{(0)}}{dt} = 2\mathbb{B}. \quad (\text{A.3})$$

An expression for $\nabla_i t_*$ may be derived, using the fact that $V^{(1)}(\phi; \mu_*(\phi))$ identically vanishes:

$$V^{(1)}(\phi; \mu_*(\phi)) = \mathbb{A}(\phi; \mu_*(\phi)) + \mathbb{B}(\phi; \mu_*(\phi)) \log \frac{\varphi^2}{\mu_*^2} = 0 \quad \forall \phi. \quad (\text{A.4})$$

Taking the field derivatives of the previous equation yields (we temporarily omit the functions' arguments for clarity):

$$\begin{aligned} \nabla_i V^{(1)} &= \nabla_i \mathbb{A} + \nabla_i \mathbb{B} \log \frac{\varphi^2}{\mu_*^2} + 2\mathbb{B} \left(\frac{\phi^i}{\varphi^2} - 2\nabla_i t_* \right) = 0 \\ \Rightarrow \quad \nabla_i t_* &= \frac{\phi^i}{\varphi^2} + \frac{1}{2\mathbb{B}} \left(\nabla_i \mathbb{A} + \nabla_i \mathbb{B} \log \frac{\varphi^2}{\mu_*^2} \right). \end{aligned} \quad (\text{A.5})$$

Neglecting terms of order 2 in perturbation theory, the field derivatives of \mathbb{A} and \mathbb{B} can be simplified as ¹³

$$\nabla_i \mathbb{A} = \frac{\partial \mathbb{A}}{\partial \phi^i} + \nabla_i t_* \frac{d\mathbb{A}}{dt} \approx \frac{\partial \mathbb{A}}{\partial \phi^i}, \quad (\text{A.6})$$

$$\nabla_i \mathbb{B} = \frac{\partial \mathbb{B}}{\partial \phi^i} + \nabla_i t_* \frac{d\mathbb{B}}{dt} \approx \frac{\partial \mathbb{B}}{\partial \phi^i}. \quad (\text{A.7})$$

In this approximation, it is straightforward to derive the radial stationary point equation (A.9), by first noting that

$$\begin{aligned} \phi^i \nabla_i t_* &= 1 + \frac{1}{2\mathbb{B}} \left(\phi^i \frac{\partial \mathbb{A}}{\partial \phi^i} + \phi^i \frac{\partial \mathbb{B}}{\partial \phi^i} \log \frac{\varphi^2}{\mu_*^2} \right) \\ &= 1 + \frac{1}{2\mathbb{B}} 4V^{(1)} = 1, \end{aligned} \quad (\text{A.8})$$

where the last line stems from the homogeneity of \mathbb{A} and \mathbb{B} with respect to ϕ . Hence, we may write

$$\phi^i \nabla_i V^{\text{eff}} = \phi^i \frac{\partial V^{\text{eff}}}{\partial \phi^i} + 2\mathbb{B} \phi^i \nabla_i t_* = 4V^{\text{eff}} + 2\mathbb{B} = 0, \quad (\text{A.9})$$

which is the radial stationary point equation derived in [18]. Going one step further, it is possible to reiterate the derivation beyond the one-loop approximation. We first derive the exact form of $\nabla_i t_*$, starting from Eq. (A.5) and using once again the decomposition (A.1):

$$\begin{aligned} \nabla_i t_* &= \frac{\phi^i}{\varphi^2} + \frac{1}{2\mathbb{B}} \left(\nabla_i \mathbb{A} + \nabla_i \mathbb{B} \log \frac{\varphi^2}{\mu_*^2} \right) \\ &= \frac{\phi^i}{\varphi^2} + \frac{1}{2\mathbb{B}} \left(\frac{\partial \mathbb{A}}{\partial \phi^i} + \frac{\partial \mathbb{B}}{\partial \phi^i} \log \frac{\varphi^2}{\mu_*^2} \right) + \frac{1}{2\mathbb{B}} \nabla_i t_* \left(\frac{d\mathbb{A}}{dt} + \frac{d\mathbb{B}}{dt} \log \frac{\varphi^2}{\mu_*^2} \right). \end{aligned} \quad (\text{A.10})$$

Collecting all the $\nabla_i t_*$ terms in the left-hand side, one finally gets

$$\nabla_i t_* = \eta \left[\frac{\phi^i}{\varphi^2} + \frac{1}{2\mathbb{B}} \left(\frac{\partial \mathbb{A}}{\partial \phi^i} + \frac{\partial \mathbb{B}}{\partial \phi^i} \log \frac{\varphi^2}{\mu_*^2} \right) \right] \quad (\text{A.11})$$

where

$$\eta \equiv \left[1 - \frac{1}{2\mathbb{B}} \left(\frac{d\mathbb{A}}{dt} + \frac{d\mathbb{B}}{dt} \log \frac{\varphi^2}{\mu_*^2} \right) \right]^{-1}. \quad (\text{A.12})$$

In other words, including the order 2 contributions introduces a multiplicative factor η in the expression of $\nabla_i t_*$, satisfying

$$\eta = 1 + \mathcal{O}(\hbar^2). \quad (\text{A.13})$$

In particular, the set of stationary point equations now reads

$$\nabla_i V^{\text{eff}} = \partial_i V^{\text{eff}} + 2\eta \mathbb{B} \nabla_i t_* = 0, \quad (\text{A.14})$$

¹³This is the $t_*^{(0)}$ approximation mentioned in [17, 18].

and the radial stationary point equation becomes

$$4V^{\text{eff}} + 2\eta\mathbb{B} = 0. \quad (\text{A.15})$$

Clearly, in the $O(\hbar)$ approximation where the running of \mathbb{A} and \mathbb{B} is neglected, (A.15) reduces to (A.9):

$$4V^{\text{eff}} + 2\mathbb{B} = 0. \quad (\text{A.16})$$

The main advantage of the above approximation is that Eq. (A.16) always takes a polynomial form in the fields. More precisely, the quantity

$$\tilde{V}^{(0)} \equiv V^{\text{eff}} + \frac{1}{2}\mathbb{B} \quad (\text{A.17})$$

takes the same polynomial form as $V^{(0)}$ with 1-loop corrected numerical coefficients and vanishes at a minimum by (A.9). It can be shown [18] that the second derivative of the potential along the radial direction is proportional to \mathbb{B} . Therefore, according to (A.9), at a minimum one has $\mathbb{B} > 0$ and $V^{\text{eff}} < 0$.

A.2 RG-improvement and the Gildener-Weinberg approximation

In the Gildener-Weinberg approach [38], the renormalisation scale prescription consists in identifying the RG-scale μ_{GW} at which the tree-level potential develops a flat direction. Along this flat direction, the field values are expressed as

$$\phi = \varphi \vec{n}. \quad (\text{A.18})$$

Based on the general expression of the one loop contributions to the scalar potential (3.1) and on the homogeneity of \mathbb{A} and \mathbb{B} with respect to the radial coordinate, one may write

$$V^{(1)}(\phi; \mu) = \mathbb{A}(\phi; \mu) + \mathbb{B}(\phi; \mu) \log \frac{\varphi^2}{\mu^2} = \mathbb{A}(\vec{n}; \mu) \varphi^4 + \mathbb{B}(\vec{n}; \mu) \varphi^4 \log \frac{\varphi^2}{\mu^2} \quad (\text{A.19})$$

so the tree-level and 1-loop contributions to the scalar potential take the following form along the flat direction:

$$V^{(0)}(\phi; \mu_{\text{GW}}) = \lambda(\vec{n}; \mu_{\text{GW}}) \varphi^4 = 0, \quad (\text{A.20})$$

$$V^{(1)}(\phi; \mu_{\text{GW}}) = \mathbb{A}(\vec{n}; \mu_{\text{GW}}) \varphi^4 + \mathbb{B}(\vec{n}; \mu_{\text{GW}}) \varphi^4 \log \frac{\varphi^2}{\mu_{\text{GW}}^2}. \quad (\text{A.21})$$

Taking the derivative with respect to φ yields

$$\frac{\partial V^{(0)}}{\partial \varphi}(\phi; \mu_{\text{GW}}) = 4\lambda(\vec{n}; \mu_{\text{GW}}^2) \varphi^3 = 0, \quad (\text{A.22})$$

$$\frac{\partial V^{(1)}}{\partial \varphi}(\phi; \mu_{\text{GW}}) = 4\varphi^3 \left[\mathbb{A}(\vec{n}; \mu_{\text{GW}}) + \mathbb{B}(\vec{n}; \mu_{\text{GW}}) \left(\log \frac{\varphi^2}{\mu_{\text{GW}}^2} + \frac{1}{2} \right) \right]. \quad (\text{A.23})$$

Hence at the minimum the radial coordinate satisfies the relation

$$\log \frac{\langle \varphi \rangle^2}{\mu_{\text{GW}}^2} = -\frac{1}{2} - \frac{\mathbb{A}}{\mathbb{B}}. \quad (\text{A.24})$$

Getting back to the RG improvement procedure described in section 3.1, one may define a RG-scale $\tilde{\mu}$ such that the one loop corrections vanish at the field value $\langle\phi\rangle = \vec{n}\langle\varphi\rangle$, namely:

$$V^{(1)}(\langle\phi\rangle; \tilde{\mu}) = 0. \quad (\text{A.25})$$

Let $\delta t = \tilde{t} - t_{\text{GW}} = \log \frac{\tilde{\mu}^2}{\mu_{\text{GW}}^2}$ be the associated shift in the logarithm of the RG-scales. To first order in δt , one has

$$V^{(0)}(\langle\phi\rangle, \tilde{\mu}) = V^{(0)}(\langle\phi\rangle, \mu_{\text{GW}}) + \delta t \frac{dV^{(0)}}{dt}(\langle\phi\rangle, \mu_{\text{GW}}) + \mathcal{O}(\delta t^2), \quad (\text{A.26})$$

$$\mathbb{A}(\vec{n}, \tilde{\mu}) = \mathbb{A}(\vec{n}, \mu_{\text{GW}}) + \delta t \frac{d\mathbb{A}}{dt}(\vec{n}, \mu_{\text{GW}}) + \mathcal{O}(\delta t^2), \quad (\text{A.27})$$

$$\mathbb{B}(\vec{n}, \tilde{\mu}) = \mathbb{B}(\vec{n}, \mu_{\text{GW}}) + \delta t \frac{d\mathbb{B}}{dt}(\vec{n}, \mu_{\text{GW}}) + \mathcal{O}(\delta t^2). \quad (\text{A.28})$$

Discarding terms that are formally of order 2 in perturbation theory allows to simplify the last two relations:

$$\mathbb{A}(\vec{n}, \tilde{\mu}) = \mathbb{A}(\vec{n}, \mu_{\text{GW}}) + \mathcal{O}(\delta t^2), \quad (\text{A.29})$$

$$\mathbb{B}(\vec{n}, \tilde{\mu}) = \mathbb{B}(\vec{n}, \mu_{\text{GW}}) + \mathcal{O}(\delta t^2). \quad (\text{A.30})$$

Had we retained terms of order $(\delta t)^2$ in the above expansions, working in the 1-loop approximation would have yielded Eqs. (A.26), (A.29), (A.30) anyways, since the $\mathcal{O}(\delta t^2)$ terms formally encompass $\mathcal{O}(\hbar^2)$ quantities. Combining Eqs. (A.23) and (A.29), (A.30) allows to rewrite the Gildener-Weinberg radial stationary point equation at the shifted scale $\tilde{\mu}$:

$$\begin{aligned} 0 &= \frac{\partial}{\partial\varphi} \left(V^{(0)}(\phi; \mu_{\text{GW}}) + V^{(1)}(\phi; \mu_{\text{GW}}) \right) \\ &= 4\varphi^3 \left[\mathbb{A}(\vec{n}, \tilde{\mu}) + \mathbb{B}(\vec{n}; \tilde{\mu}) \left(\log \frac{\varphi^2}{\tilde{\mu}^2} + 2\delta t + \frac{1}{2} \right) \right] \\ &= 4\varphi^3 \mathbb{B}(\vec{n}; \tilde{\mu}) \left(\frac{1}{2} + 2\delta t \right), \end{aligned} \quad (\text{A.31})$$

where Eq. (A.25) was used in the last step. We conclude that, in the one loop approximation,

$$\delta t = -\frac{1}{4}. \quad (\text{A.32})$$

Considering the first order truncation of Callan-Symanzik equation (3.7),

$$\frac{dV^{(0)}}{dt} = 2\mathbb{B}. \quad (\text{A.33})$$

we finally obtain the relation

$$V^{(0)}(\phi; \mu_{\text{GW}}) = V^{(0)}(\phi; \tilde{\mu}) - 2\mathbb{B}(\phi; \mu_{\text{GW}})\delta t = V^{(0)}(\phi; \tilde{\mu}) + \frac{1}{2}\mathbb{B}(\phi; \tilde{\mu}) \equiv \tilde{V}^{(0)}(\phi; \tilde{\mu}), \quad (\text{A.34})$$

where the quantity $\tilde{V}^{(0)}$ is defined similarly as in Eq. (A.17). Quite importantly, the above relation implies that in the one loop approximation, at the scale $\tilde{\mu}$, the corrected tree-level

potential $\tilde{V}^{(0)}$ has the same structure than the tree-level potential evaluated at the scale μ_{GW} . In particular, $\tilde{V}^{(0)}(\phi; \tilde{\mu})$ inherits the flat direction of $V^{(0)}(\phi; \mu_{\text{GW}})$, and therefore

$$\tilde{V}^{(0)}(\langle\phi\rangle; \tilde{\mu}) = 0. \quad (\text{A.35})$$

From the above equation, we may finally conclude that the Gildener-Weinberg vev $\langle\phi\rangle$ satisfies the RG-improved radial stationary point equation (A.9). It is worth emphasising that, $\langle\phi\rangle$ is not, in general, a solution of the full set of stationary point equations (A.2), *i.e.* it does not minimise the RG-improved potential V^{eff} . In what follows, we will show however that it constitutes a first order approximation of the actual vev $\langle\phi\rangle^{\text{min}}$.

Denoting $\delta\phi = \langle\phi\rangle^{\text{min}} - \langle\phi\rangle$ the shift between the actual vev and the Gildener-Weinberg solution, one may write, to first order in $\delta\phi$:

$$\tilde{V}^{(0)}(\langle\phi\rangle^{\text{min}}) = \tilde{V}^{(0)}(\langle\phi\rangle) + \delta\phi^i \nabla_i \tilde{V}^{(0)}(\langle\phi\rangle) + \mathcal{O}(\delta\phi^2). \quad (\text{A.36})$$

Since both $\langle\phi\rangle^{\text{min}}$ and $\langle\phi\rangle$ belong to the hypersurface where the radial stationary point equation is satisfied (*i.e.* where $V^{\text{eff}} = 0$) and using the decomposition (A.1), the above relation reduces to

$$0 = \delta\phi^i \nabla_i \tilde{V}^{(0)}(\langle\phi\rangle) = \delta\phi^i \partial_i \tilde{V}^{(0)}(\langle\phi\rangle) + \delta\phi^i \nabla_i t_* (\langle\phi\rangle) \frac{d\tilde{V}^{(0)}}{dt}(\langle\phi\rangle). \quad (\text{A.37})$$

The ∂_i derivative in the right-hand side of the above equation vanishes since $\langle\phi\rangle$ lies along the flat direction of $\tilde{V}^{(0)}(\phi; \tilde{\mu})$. In addition, to first order in perturbation theory, one can approximate

$$\frac{d\tilde{V}^{(0)}}{dt}(\langle\phi\rangle) = \frac{dV^{(0)}}{dt}(\langle\phi\rangle) + \mathcal{O}(\hbar^2), \quad (\text{A.38})$$

and (A.37) implies

$$\delta\phi^i \nabla_i t_* (\langle\phi\rangle) = 0. \quad (\text{A.39})$$

Furthermore, to first order in $\delta\phi^i$

$$t_*(\langle\phi\rangle^{\text{min}}) = t_*(\langle\phi\rangle) + \delta\phi^i \nabla t_* (\langle\phi\rangle), \quad (\text{A.40})$$

so we can finally establish that, to first order in perturbation theory,

$$t_*(\langle\phi\rangle^{\text{min}}) = t_*(\langle\phi\rangle) + \mathcal{O}(\delta\phi^2) \quad \Rightarrow \quad \mu_*^{\text{min}} \approx \tilde{\mu}. \quad (\text{A.41})$$

The above approximation constitutes the main result of this appendix, which can be summarised as follows: The RG-scale $\tilde{\mu}$ at which the corrected tree-level potential $\tilde{V}^{(0)} = V^{(0)} + \mathbb{B}/2$ develops a flat direction is a first order approximation of the value taken by field-dependent RG-scale μ_*^{min} at the minimum of the RG-improved potential. This observation justifies the procedure described in section 3.2 to estimate, in an algorithmically efficient way, the position and depth of the minimum of the RG-improved potential.

A.3 Minimisation beyond the one-loop approximation

The numerical procedure described in section 3.2 in the one-loop approximation of the radial stationary point equation can be slightly improved by taking into account corrections that are formally of order 2 in perturbation theory. For convenience, we rewrite below the exact radial stationary point equation (A.15) obtained beyond the 1-loop approximation:

$$4V^{(0)} + 2\eta\mathbb{B} = 0. \quad (\text{A.42})$$

where

$$\eta = \left[1 - \frac{1}{2\mathbb{B}} \left(\frac{d\mathbb{A}}{dt} + \frac{d\mathbb{B}}{dt} \log \frac{\varphi^2}{\mu_*^2} \right) \right]^{-1}. \quad (\text{A.43})$$

The expression of η can be further simplified by using

$$V^{(1)} = \mathbb{A} + \mathbb{B} \log \frac{\varphi^2}{\mu_*^2} = 0 \quad \Rightarrow \quad \log \frac{\varphi^2}{\mu_*^2} = -\frac{\mathbb{A}}{\mathbb{B}}, \quad (\text{A.44})$$

namely:

$$\eta = \left[1 - \frac{1}{2} \frac{\frac{d\mathbb{A}}{dt}\mathbb{B} - \mathbb{A}\frac{d\mathbb{B}}{dt}}{\mathbb{B}^2} \right]^{-1} = \left[1 - \frac{1}{2} \frac{d}{dt} \frac{\mathbb{A}}{\mathbb{B}} \right]^{-1}. \quad (\text{A.45})$$

In this latter form, it is clear that η does not depend on the radial field coordinate, but only on the direction of the field vector in the field space. We conveniently make use of this property in an iterative method allowing to estimate the position of the minimum beyond the 1-loop approximation. We restate below the minimisation procedure described in Section 3.2, where steps 3 and 4 have been modified to include the effect of 2-loop corrections stemming from η , namely:

1. Starting with random values for the quartic couplings at some high scale μ_0 , the stability of the tree-level potential is asserted, and unstable configurations are discarded.
2. Evolution of the quartic couplings according to their RG running is performed down to some lower scale μ_1 .
3. At this point, we initialise the iterative procedure taking into account the effects of $\eta \neq 1$. For the first iteration, we set

$$k = 0, \quad \eta_k = \eta_0 = 1.$$

Defining

$$\tilde{V}^{(0)} \Big|_k = \tilde{V}^{(0)} \Big|_{\eta=\eta_k} = V^{(0)} + 2\eta_k\mathbb{B},$$

the scale $\tilde{\mu}_k$ at which $\tilde{V}^{(0)} \Big|_k$ develops flat directions is identified.

4. At the scale $\tilde{\mu}_k$, the flat direction \vec{n}_k is identified. The value of

$$\eta_{k+1} = \eta(\vec{n}_k; \tilde{\mu}_k)$$

does not depend on the radial field coordinate, and is evaluated using Eq. (A.45). If $|\eta_{k+1} - \eta_k| > \varepsilon$, we repeat step 3 with

$$k \rightarrow k + 1, \quad \eta_k \rightarrow \eta_{k+1}.$$

Otherwise, we consider that the iteration has converged (in practice we set $\varepsilon = 10^{-5}$), and will use $\vec{n} = \vec{n}_k$ as the corrected generating vector of the flat direction, along which the field values take the form

$$\phi = \varphi \vec{n}.$$

5. The unique value of $\langle \varphi \rangle$ such that

$$V^{(1)}(\langle \varphi \rangle \vec{n}; \tilde{\mu}) = 0$$

is identified. The field vector $\langle \phi \rangle = \langle \varphi \rangle \vec{n}$ constitutes an estimation of the exact position of the minimum.

6. Finally, the depth of the RG-improved potential at the minimum, *i.e.* the quantity

$$V^{\text{eff}}(\langle \phi \rangle) = V^{(0)}(\langle \phi \rangle; \tilde{\mu})$$

is evaluated.

This modified minimisation procedure allows to achieve better accuracy (see the next section) on the estimation of the position and depth of the minimum. This is the procedure that was systematically used in our numerical study of the breaking patterns of the model.

A.4 Numerical performance and accuracy of the minimisation procedure

In order to confirm that the simplified minimisation procedure described in Section 3.2 and improved above does provide a reasonable estimation of the depth and position of the minimum, we have compared its outcome with that of a full-fledged numerical minimisation of the RG-improved potential. This comparison has been performed on a random sample of points, both in the case of 2- and 3-vev manifolds¹⁴, for which the number of minima hence characterised amounts to $N^{(2)} = 2000$ and $N^{(3)} = 500$, respectively.

As stated before, the main motivation for using a simplified minimisation procedure is to speed-up the computations, therefore enabling one to perform a random scan over a large sample of points. Fig. A.1 illustrates the performance improvement in terms of execution time for both 2- and 3-vev manifolds. Given a minimum, we define T_{full} as the execution time of a full numerical minimisation and T_{simp} as the execution time of the simplified algorithms. The gain in performance $T_{\text{full}}/T_{\text{simp}}$ is of order $\mathcal{O}(10^2)$ and $\mathcal{O}(10^3)$ –

¹⁴By construction, the improved minimisation procedure described above is ensured to converge towards the true minimum in the case of 1-vev manifolds.

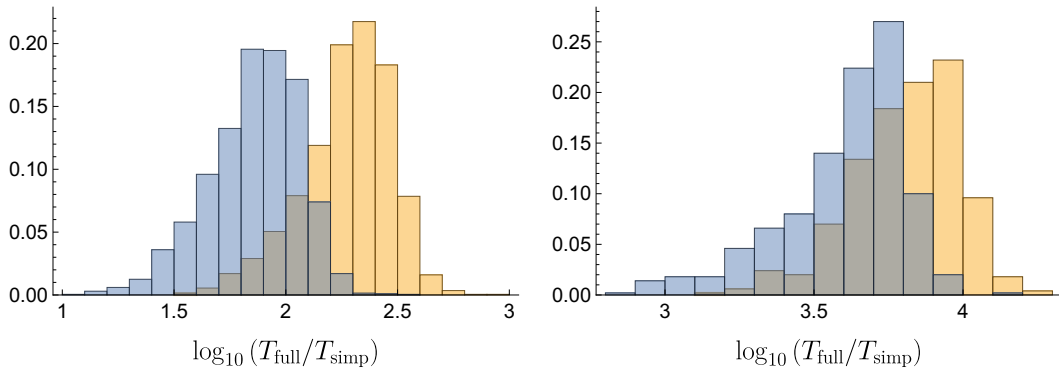


Figure A.1: Gain in performance for 2-vev (left panel) and 3-vev (right panel) manifolds, using the minimisation procedure described in Section 3.2 (yellow bars) and its improved version (blue bars), compared to a full-fledged numerical minimisation.

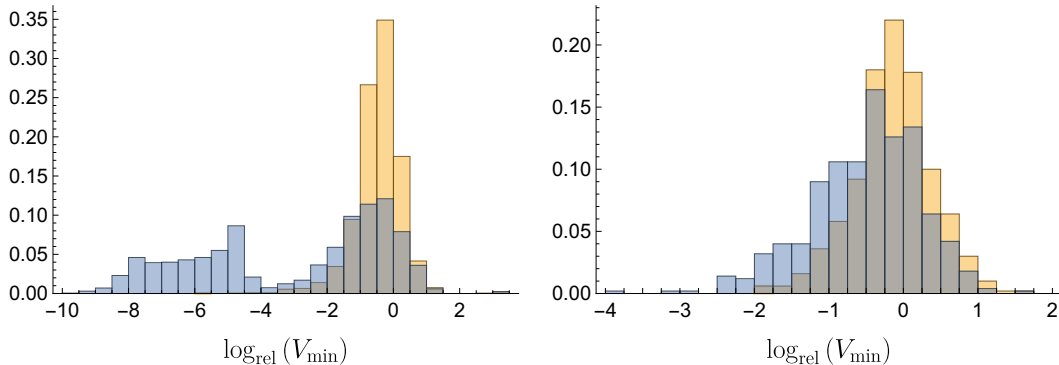


Figure A.2: Logarithmic relative error on V_{\min} for 2-vev (left panel) and 3-vev (right panel) manifolds, using the minimisation procedure described in Section 3.2 (yellow bars) and its improved version (blue bars), compared to a full-fledged numerical minimisation.

$\mathcal{O}(10^4)$ for 2- and 3-vev manifolds respectively. Note that, on the computer used to perform this analysis, the average execution time of the full numerical minimisation is 4 s for 2-vev manifolds and 460 s for 3-vev manifolds.

Of course, the major gain in performance comes at a price: our minimisation procedure only provides an approximation of the position and depth of a minimum. However, as shown in Figures A.2–A.4, the relative error on the quantities V_{\min} , $\varphi^{\min} = \sqrt{\langle \phi \rangle_i^{\min} \langle \phi \rangle_i^{\min}}$ and $t_*^{\min} = t_*(\langle \phi \rangle^{\min})$ are kept at a reasonable level. Concretely speaking, defining the logarithmic relative error on the parameter X (with $X = V_{\min}, \varphi^{\min}, t_*^{\min}$) as

$$\log_{\text{rel}}(X) = \log_{10} |\delta(X)| = \log_{10} \left| 100 \times \frac{X_{\text{simp}} - X_{\text{full}}}{X_{\text{full}}} \right|, \quad (\text{A.46})$$

rare are the points for which $\log_{\text{rel}}(X) > 1$. In other words, the relative error (in particular on the depth of the potential at a minimum, which is the most important quantity in this

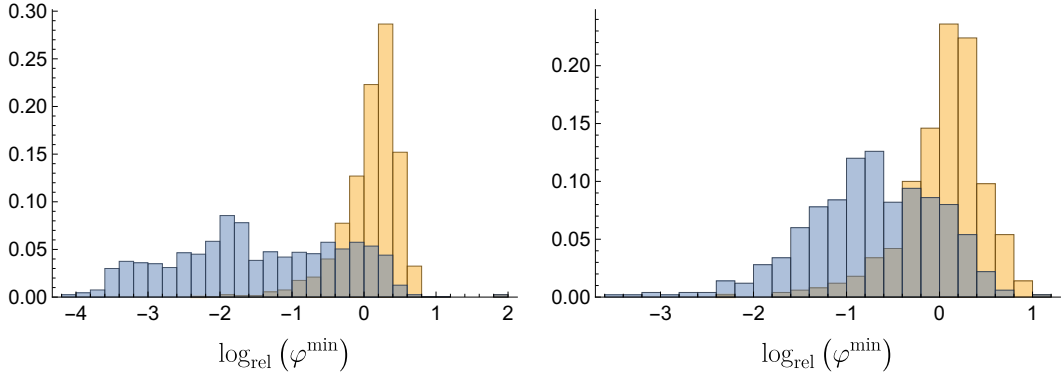


Figure A.3: Logarithmic relative error on φ^{\min} for 2-vev (left panel) and 3-vev (right panel) manifolds, using the minimisation procedure described in Section 3.2 (yellow bars) and its improved version (blue bars), compared to a full-fledged numerical minimisation.

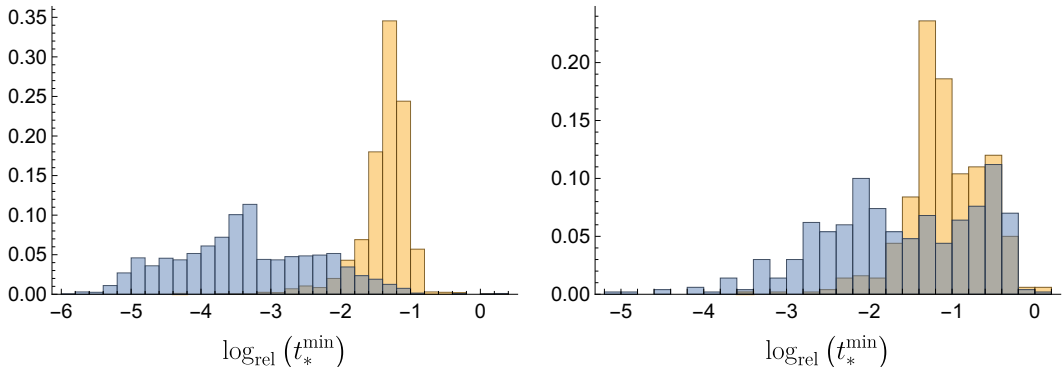


Figure A.4: Logarithmic relative error on t_*^{\min} for 2-vev (left panel) and 3-vev (right panel) manifolds, using the minimisation procedure described in Section 3.2 (yellow bars) and its improved version (blue bars), compared to a full-fledged numerical minimisation.

analysis) is almost always kept under the 10% level. In fact, focusing on the quantity of interest, V_{\min} , we observe that:

- For 2-vev manifolds, $\delta(V_{\min}) > 10\%$ for 0.8% of the points and $\delta(V_{\min}) > 5\%$ for 2.4% of the points,
- For 3-vev manifolds, $\delta(V_{\min}) > 10\%$ for 0.6% of the points and $\delta(V_{\min}) > 5\%$ for 3% of the points.

In addition, two comments are worth making regarding the left panel of Fig. A.2, showing the relative error on V_{\min} in the case of 2-vev manifolds:

- The excess of points with a relative error of order $\mathcal{O}(10^{-10}\%)$ to $\mathcal{O}(10^{-4}\%)$ corresponds to situations where one of the two vevs actually vanishes along the flat direction. In such cases, one effectively ends up minimising a 1-vev manifold, for

which the improved minimisation procedure in ensured to converge towards the true minimum (up to numerical errors).

- A small number of points (5 out of 2000) give $\log_{\text{rel}}(V_{\text{min}}) \approx 3$ or, equivalently, $\delta(V_{\text{min}}) \approx 1000\%$. We have explicitly checked that those points are in fact characterised by the occurrence of two flat directions of different nature at RG-scales very close to each other, implying in turn the existence of two distinct local minima. Hence, the large value of the relative error is simply explained by the fact that the full numerical minimisation has converged in this case towards one of the two minima, distinct from the one characterised by the simplified minimisation algorithm.

Finally, Figures A.2–A.4 show that, as expected, the improved minimisation algorithm described in App. A.3 overall yields a better characterisation of the minima, both in the case of 2- and 3-vev manifolds (at the reasonable cost of a slightly increased execution time).

B General tree-level stability conditions

The various breaking patterns studied in this work are characterised by vacuum manifolds consisting of at most 3 vevs. In this appendix, we establish the conditions of tree-level stability for general potentials of 1, 2 and 3 variables, as well as the circumstances of their violation along the RG-flow. We give in particular a characterisation of the flat directions that appear at the precise energy scale at which the violation of tree-level stability occurs.

For completeness, let us start the discussion with 1-vev vacuum manifolds (occurring for instance in the $SO(8) \times U(1)$ breaking), for which the study of stability and its violation is trivial. Such a vacuum structure is parametrised by

$$V(x) = ax^4, \tag{B.1}$$

so the condition for a stable (*i.e.* bounded from below) potential is simply

$$a > 0. \tag{B.2}$$

Therefore, symmetry breaking will be uniquely triggered along the RG-flow as soon as the quartic coupling a turns negative.

B.1 Stability of 2-vev vacuum manifolds

Now turning to vacuum manifolds consisting of 2 variables, we have in general:

$$V(x, y) = a_0x^4 + a_1x^2y^2 + a_2y^4, \tag{B.3}$$

and it is straightforward to derive the conditions of a stable potential:

$$a_0 > 0 \wedge a_2 > 0 \wedge a_1 + 2\sqrt{a_0a_2} > 0. \tag{B.4}$$

Following the discussion in Sec. 4.2, the stability constraints can be violated in three distinct manners, corresponding to the violation of any one of the three conditions in Eq. (B.4).

Below we examine the generated flat direction in each of these three cases. We make the assumption that only one of the three conditions in Eq. (B.4) gets violated along the RG-flow, *i.e.* that the other two remain satisfied.

Case 1: $a_0 = 0$. The potential simplifies as

$$V(x, y) = (a_1 x^2 + a_2 y^2) y^2, \quad (\text{B.5})$$

and the other stability constraints are satisfied, namely

$$a_2 > 0 \wedge a_1 > 0. \quad (\text{B.6})$$

Clearly, the flat direction is parameterised by

$$\begin{pmatrix} x \\ y \end{pmatrix} = \lambda \begin{pmatrix} 1 \\ 0 \end{pmatrix}, \quad \lambda \in \mathbb{R}. \quad (\text{B.7})$$

Case 2: $a_2 = 0$. Similarly, the potential simplifies as

$$V(x, y) = (a_0 x^2 + a_1 y^2) x^2, \quad (\text{B.8})$$

and since $a_0, a_1 > 0$, the flat direction occurs in the direction

$$\begin{pmatrix} x \\ y \end{pmatrix} = \lambda \begin{pmatrix} 0 \\ 1 \end{pmatrix}. \quad (\text{B.9})$$

Case 3: $a_1 + 2\sqrt{a_0 a_2} = 0$. In this case, the potential can be factored in the form

$$V(x, y) = (\sqrt{a_0} x^2 - \sqrt{a_2} y^2)^2. \quad (\text{B.10})$$

The other constraints are satisfied, namely

$$a_0 > 0 \wedge a_2 > 0, \quad (\text{B.11})$$

and two flat directions occur in the directions

$$\begin{pmatrix} x \\ y \end{pmatrix} = \lambda \begin{pmatrix} a_2^{1/4} \\ \pm a_0^{1/4} \end{pmatrix}. \quad (\text{B.12})$$

B.2 Stability of 3-vev vacuum manifolds

We finally turn to the study of 3-vev manifolds, which will need a much more elaborate discussion. However it will be helpful to note that the 3-vev structures considered in this work can be put in the form

$$V(\chi, \omega_1, \omega_2) = \alpha \chi^4 + \beta(\omega_1, \omega_2) \chi^2 + \gamma(\omega_1, \omega_2), \quad (\text{B.13})$$

where β and γ take the general forms

$$\beta(\omega_1, \omega_2) = b_0\omega_1^2 + b_1\omega_1\omega_2 + b_2\omega_2^2 = (b_0 + b_1X + b_2X^2)\omega_1^2 = \tilde{\beta}(X)\omega_1^2, \quad (\text{B.14})$$

$$\gamma(\omega_1, \omega_2) = c_0\omega_1^4 + c_1\omega_1^2\omega_2^2 + c_2\omega_2^4 = (c_0 + c_1X^2 + c_2X^4)\omega_1^4 = \tilde{\gamma}(X)\omega_1^4, \quad (\text{B.15})$$

with $X = \omega_2/\omega_1$. For the above potential to be bounded from below, it must be non-negative for all values of the vevs. First of all, positivity at $\omega_1 = \omega_2 = 0$ and at $\chi = 0$ imposes the constraints

$$\alpha > 0 \wedge \gamma(\omega_1, \omega_2) > 0, \quad \forall(\omega_1, \omega_2). \quad (\text{B.16})$$

Reusing the results established above for 2-vev functions, the latter inequality requires

$$c_0 > 0 \wedge c_2 > 0 \wedge c_1 + 2\sqrt{c_0c_2} > 0. \quad (\text{B.17})$$

Then, taking V as a quadratic polynomial in χ^2 , positivity requires its roots to be either complex or negative. Defining¹⁵ $\Delta = 4\alpha\gamma - \beta^2$, the condition to have either complex roots or non-positive roots reads

$$\Delta(\omega_1, \omega_2) > 0 \vee \left(\Delta(\omega_1, \omega_2) \leq 0 \wedge \beta(\omega_1, \omega_2) > 0 \right), \quad \forall(\omega_1, \omega_2), \quad (\text{B.18})$$

or, more concisely

$$\Delta(\omega_1, \omega_2) > 0 \vee \beta(\omega_1, \omega_2) > 0, \quad \forall(\omega_1, \omega_2). \quad (\text{B.19})$$

The quantity $\Delta(\omega_1, \omega_2)$ can be generically expressed as

$$\begin{aligned} \Delta(\omega_1, \omega_2) &= 4\alpha\gamma(\omega_1, \omega_2) - \beta(\omega_1, \omega_2)^2 \\ &= a_0\omega_1^4 + a_1\omega_1^3\omega_2 + a_2\omega_1^2\omega_2^2 + a_3\omega_1\omega_2^3 + a_4\omega_2^4 \\ &= (a_0 + a_1X + a_2X^2 + a_3X^3 + a_4X^4)\omega_1^4 \\ &= \tilde{\Delta}(X)\omega_1^4, \end{aligned} \quad (\text{B.20})$$

and in practice, when $\omega_2 \neq 0$, one only needs to consider the simplified stability constraint

$$\tilde{\Delta}(X) > 0 \vee \tilde{\beta}(X) > 0, \quad \forall X. \quad (\text{B.21})$$

Since $\tilde{\beta}$ and $\tilde{\Delta}(X)$ are polynomials of respective degree 2 and 4 in X , one could determine analytic conditions for them to be positive for all X . However, we insist that the constraint (B.21) is *not* equivalent to the following:

$$\left(\tilde{\Delta}(X) > 0, \quad \forall X \right) \vee \left(\tilde{\beta}(X) > 0, \quad \forall X \right), \quad (\text{B.22})$$

since the latter is only a sufficient condition for the former to be satisfied. Instead, one should simultaneously inspect the shape of both polynomials in terms of their number of real roots and the sign of their leading coefficient, in order to identify the regions where either

¹⁵Note the negative sign compared to the usual definition of the quadratic discriminant.

one or the other is positive. Such a case-by-case study is readily performed, as reported in Table B.1. Here, since we aim at determining the conditions of a stable potential (B.13), we will consider that all other necessary conditions determined previously must hold. In particular, (B.16) holds. Hence, a useful observation to make is that if $\tilde{\beta} = 0$, then

$$\tilde{\Delta}(X) = 4\alpha\tilde{\gamma}(X) > 0. \quad (\text{B.23})$$

In other words, $\tilde{\Delta}(X)$ is always strictly positive at the locations of the roots of $\tilde{\beta}$. This greatly reduces the number of possibilities when inspecting the shapes of the two polynomials. Overall, $\tilde{\Delta}$ can have either 0, 2 or 4 real roots, with a positive or negative leading coefficient a_4 , while $\tilde{\beta}$ can have either 0 or 2 real roots with a positive or negative leading coefficient b_2 . At this point, a comment is worth making: we do not consider the cases of multiple roots, nor those of a vanishing leading coefficient. The reason is that, at the initial scale where potential stability must be asserted, the couplings (and therefore the value of the coefficients appearing in the polynomials) are generated randomly. Hence, exact relations such that a vanishing discriminant or coefficient will never occur. On the other hand, such quantities can very well vanish at a given scale along the RG-flow and possibly trigger spontaneous breaking of the model. Such situations are described in subsection B.3 below.

Table B.1: Realisation of the stability constraint (B.21), depending on the number of roots of the polynomials $\tilde{\Delta}$ and $\tilde{\beta}$ and the sign of their leading coefficient. We write $\Delta(n)^s$ and $\beta(n)^s$ to respectively denote the number n of roots and the sign s of the leading coefficient of the polynomials $\tilde{\Delta}$ and $\tilde{\beta}$. The roots of $\tilde{\Delta}$ are noted δ_i with $\delta_1 < \dots < \delta_n$, those of $\tilde{\beta}$ are noted β_i with $\beta_1 < \beta_2$. Cases where the stability condition (B.21) is satisfied for any values of the roots are referred to as Stable, and cases where the condition cannot be satisfied are referred to as Unstable. For cases where the realisation of (B.21) depends on the value of the roots, the additional constraints to be satisfied by them are reported. Finally, two cases never occur because of the constraint of a positive $\tilde{\Delta}$ at the location of the roots of $\tilde{\beta}$.

	$\beta(0)^+$	$\beta(0)^-$	$\beta(2)^+$	$\beta(2)^-$
$\Delta(0)^+$	Stable	Stable	Stable	Stable
$\Delta(0)^-$	Stable	Unstable	/	/
$\Delta(2)^+$	Stable	Unstable	$\beta_2 < \delta_1 \vee \beta_1 > \delta_2$	$\beta_2 < \delta_1 \wedge \beta_1 > \delta_2$
$\Delta(2)^-$	Stable	Unstable	$\beta_1 > \delta_1 \wedge \beta_2 < \delta_2$	Unstable
$\Delta(4)^+$	Stable	Unstable	$\beta_2 < \delta_1 \vee \beta_1 > \delta_4 \vee (\beta_1 > \delta_2 \wedge \beta_2 < \delta_3)$	$\beta_1 < \delta_1 \vee \beta_2 > \delta_4$
$\Delta(4)^-$	Stable	Unstable	$(\beta_1 > \delta_1 \wedge \beta_2 < \delta_2) \vee (\beta_1 > \delta_3 \wedge \beta_2 < \delta_4)$	Unstable

Finally, although this procedure can readily be performed numerically, we review here the analytical conditions allowing to determine the number of real roots of the quartic polynomial $\tilde{\Delta}$ [62–64]. Those conditions will also help understand how the stability condition (B.21) can be violated along the RG-flow. The main quantity of interest here is the discriminant

D of the polynomial $\tilde{\Delta}$:

$$\begin{aligned}
D = & 256a_0^3a_4^3 - 4a_1^3a_3^3 - 27a_0^2a_3^4 + 16a_0a_2^4a_4 - 6a_0a_1^2a_3^2a_4 - 27a_1^4a_4^2 \\
& - 192a_0^2a_1a_3a_4^2 - 4a_2^3(a_0a_3^2 + a_1^2a_4) + 18a_2(a_1a_3 + 8a_0a_4)(a_0a_3^2 + a_1^2a_4) \\
& + a_2^2(a_1^2a_3^2 - 80a_0a_1a_3a_4 - 128a_0^2a_4^2).
\end{aligned} \tag{B.24}$$

We will not show here the expression of D as a function of α, b_i, c_i here since it is rather lengthy. However, we make the important remark that

$$D \propto \alpha^2, \tag{B.25}$$

which will help understand the symmetry breaking patterns in the next subsection. The nature of the roots depend on the sign of D :

$$D > 0 : \text{The four roots are either all complex or all real} \tag{B.26}$$

$$D = 0 : \text{There exists multiple roots} \tag{B.27}$$

$$D < 0 : \text{Two roots are complex, the other two are real} \tag{B.28}$$

In the first case, $D > 0$, the nature of the roots can be determined by defining the following additional quantities [64]

$$Q = 8a_2a_4 - 3a_3^2, \quad R = 64a_0a_4^3 + 16a_2a_3^2a_4 - 16a_4^2(a_2^2 + a_1a_3) - 3a_3^4, \tag{B.29}$$

such that the four roots are complex if either $Q > 0$ or $R > 0$. In summary, we have:

$$D > 0 \wedge (Q > 0 \vee R > 0) : \text{No real roots} \tag{B.30}$$

$$D < 0 : \text{Two real roots} \tag{B.31}$$

$$D > 0 \wedge (Q \leq 0 \wedge R \leq 0) : \text{Four real roots} \tag{B.32}$$

B.3 Stability violation for 3-vev manifolds

As previously done in the case of 2-vev manifolds, we now inspect the different ways in which the stability conditions of 3-vev manifolds can be violated. Obviously, more cases will have to be considered here, due to the richer structure of the potential and its stability conditions.

Case 1: $\alpha = 0$. The potential simplifies as

$$V(\chi, \omega_1, \omega_2) = \beta(\omega_1, \omega_2)\chi^2 + \gamma(\omega_1, \omega_2) \tag{B.33}$$

We consider that all other stability condition are satisfied. In particular, γ is always positive, and since $\alpha = 0$, one has $\Delta(\omega_1, \omega_2) = -\beta(\omega_1, \omega_2)^2$. Therefore, according to Eq. (B.19), β is

always positive, and V can only vanish in the region where $\omega_1 = \omega_2 = 0$. In this case, the flat direction lies along

$$\begin{pmatrix} \chi \\ \omega_1 \\ \omega_2 \end{pmatrix} = \lambda \begin{pmatrix} 1 \\ 0 \\ 0 \end{pmatrix}. \quad (\text{B.34})$$

This corresponds to a symmetry breaking exclusively driven by the vev χ . Specialising this result to the SM vacuum manifold (4.7) with $\chi = \chi_5$ (or equivalently $\chi = \chi_R$) yields a breaking towards the $SU(5)$ subgroup.

Case 2: $c_0 = 0$ or $c_2 = 0$. Let us first consider the case where $c_0 = 0$. In this case, the quantity $\gamma(\omega_1, \omega_2)$ vanishes along the flat direction

$$\begin{pmatrix} \omega_1 \\ \omega_2 \end{pmatrix} = \lambda \begin{pmatrix} 1 \\ 0 \end{pmatrix}, \quad (\text{B.35})$$

and according to (B.19), $\beta(\omega_1, \omega_2) > 0$. The potential simplifies as

$$V(\chi, \omega_1, \omega_2) = (\alpha\chi^2 + \beta(\omega_1, \omega_2))\chi^2, \quad (\text{B.36})$$

and can only vanish if $\chi = 0$. Hence, the flat direction is

$$\begin{pmatrix} \chi \\ \omega_1 \\ \omega_2 \end{pmatrix} = \lambda \begin{pmatrix} 0 \\ 1 \\ 0 \end{pmatrix}. \quad (\text{B.37})$$

This is a breaking triggered by the vev ω_1 exclusively. Similarly, in the case where $c_2 = 0$, the flat direction is given by

$$\begin{pmatrix} \chi \\ \omega_1 \\ \omega_2 \end{pmatrix} = \lambda \begin{pmatrix} 0 \\ 0 \\ 1 \end{pmatrix} \quad (\text{B.38})$$

and corresponds to a breaking driven by ω_2 . Considering the SM vacuum manifold (4.7) with $\omega_1 = \omega_B$, $\omega_2 = \omega_R$ and either $\chi = \chi_5$ or $\chi = \chi_5$, the above cases respectively correspond to the $3_C 2_L 2_R 1_{B-L}$ and $4_C 2_L 1_R$ breakings.

Case 2: $c_1 + 2\sqrt{c_0 c_2} = 0$. In this case, the quantity γ has a flat direction along

$$\begin{pmatrix} \omega_1 \\ \omega_2 \end{pmatrix} = \lambda \begin{pmatrix} c_2^{1/4} \\ \pm c_0^{1/4} \end{pmatrix}. \quad (\text{B.39})$$

Here again, the potential takes the form (B.36). Therefore the flat directions are given by

$$\begin{pmatrix} \chi \\ \omega_1 \\ \omega_2 \end{pmatrix} = \lambda \begin{pmatrix} 0 \\ c_2^{1/4} \\ \pm c_0^{1/4} \end{pmatrix} \quad (\text{B.40})$$

and the breaking is driven by the vevs ω_1 and ω_2 . In the SM vacuum, this corresponds to the $3_C 2_L 1_R 1_{B-L}$ breaking¹⁶.

Case 3: $a_0 = 0$ or $a_4 = 0$. Here we consider the possibility that Eq. (B.19) gets violated, in the particular situation where the leading coefficient of either ω_1^4 or ω_2^4 vanishes along the RG-flow. Starting with the case where $a_0 = 0$, we have

$$\Delta(\omega_1, \omega_2) = (a_1\omega_1^3 + a_2\omega_1^2\omega_2 + a_3\omega_1\omega_2^2 + a_4\omega_2^3)\omega_2. \quad (\text{B.41})$$

Hence, Δ clearly vanishes when $\omega_2 = 0$. We note that other roots with $\omega_1, \omega_2 \neq 0$ may exist, but this situation is taken into account in the more general **Case 4** below. Here we restrict the discussion to the case where $\omega_2 = 0$. In this case, we have

$$a_0 = 4\alpha c_0 - b_0^2 = 0, \quad (\text{B.42})$$

$$\beta(\omega_1, 0) = b_0\omega_1^2, \quad (\text{B.43})$$

so the full potential simplifies as

$$V(\chi, \omega_1, 0) = (\sqrt{\alpha}\chi^2 \pm \sqrt{c_0}\omega_1^2)^2. \quad (\text{B.44})$$

Since $\alpha > 0$ and $c_0 > 0$, the only case yielding a flat direction corresponds to $b_0 < 0$, and hence

$$V(\chi, \omega_1, 0) = (\sqrt{\alpha}\chi^2 - \sqrt{c_0}\omega_1^2)^2. \quad (\text{B.45})$$

In this case, the flat directions are given by

$$\begin{pmatrix} \chi \\ \omega_1 \\ \omega_2 \end{pmatrix} = \lambda \begin{pmatrix} c_0^{1/4} \\ \pm \alpha^{1/4} \\ 0 \end{pmatrix}. \quad (\text{B.46})$$

Reiterating the above calculations in the case where $a_4 = 0$ yields the following flat directions

$$\begin{pmatrix} \chi \\ \omega_1 \\ \omega_2 \end{pmatrix} = \lambda \begin{pmatrix} c_0^{1/4} \\ 0 \\ \pm \alpha^{1/4} \end{pmatrix}. \quad (\text{B.47})$$

When considering the SM vacuum manifold, such flat directions correspond to a complete breaking of $SO(10)$ towards the SM, despite the fact that one of the ω_i vanishes.

Case 4. Whereas all previous cases involved only one or two of the vevs, we now turn to the possibility of violating the stability conditions in a non trivial way, where none of the vevs vanishes. Concretely, it means that condition (B.19) or, equivalently, (B.21) needs to be violated along the RG-flow, in a case where $\chi, \omega_1, \omega_2 \neq 0$. A closer look at (B.21) shows

¹⁶However, for reasons explained in Sec. 4.2.3, in this case the actual breaking direction is $SU(5) \times U(1)$ since in practice one always has $\eta = \sqrt{2/3}$.

that the transition from a stable to an unstable potential can only occur at a given value of X in the two following pictures

$$\tilde{\Delta}(X) > 0 \wedge \tilde{\beta}(X) < 0 \longrightarrow \tilde{\Delta}(X) = 0 \wedge \tilde{\beta}(X) < 0 \longrightarrow \tilde{\Delta}(X) < 0 \wedge \tilde{\beta}(X) < 0, \quad (\text{B.48})$$

$$\tilde{\Delta}(X) < 0 \wedge \tilde{\beta}(X) > 0 \longrightarrow \tilde{\Delta}(X) < 0 \wedge \tilde{\beta}(X) = 0 \longrightarrow \tilde{\Delta}(X) < 0 \wedge \tilde{\beta}(X) < 0. \quad (\text{B.49})$$

However, as mentioned before, $\tilde{\Delta}(X)$ can only be positive when evaluated a root of $\tilde{\beta}$. This observation allows to rule out the scenario (B.49), making Eq. (B.48) the only way of generating a flat direction. Furthermore, the change of sign of $\tilde{\Delta}(X)$ due to a sign flip of its leading coefficient was already covered in **Case 3** above, so we can discard this possibility. The only remaining way to achieve the transition (B.48) is for $\tilde{\Delta}$ to acquire a multiple root at some value of X . This happens when the discriminant D of $\tilde{\Delta}$ vanishes at some RG-scale. The multiple real root that appears will be denoted δ , and we have

$$X = \delta \Rightarrow \omega_2 = \delta\omega_1. \quad (\text{B.50})$$

Since $\tilde{\Delta}(\delta) = \Delta(\omega_1, \delta\omega_1) = 4\alpha\gamma(\omega_1, \delta\omega_1) - \beta(\omega_1, \delta\omega_1)^2 = 0$ and $\beta(\omega_1, \delta\omega_1) < 0$, the potential takes the form

$$V(\chi, \omega_1, \delta\omega_1) = \left(\sqrt{\alpha}\chi^2 - \sqrt{\gamma(\omega_1, \delta\omega_1)} \right)^2, \quad (\text{B.51})$$

where

$$\sqrt{\gamma(\omega_1, \delta\omega_1)} = \sqrt{c_0 + c_1\delta^2 + c_2\delta^4}\omega_1^2. \quad (\text{B.52})$$

This means in turn that the potential vanishes if

$$\chi = \pm \left(\frac{c_0 + c_1\delta^2 + c_2\delta^4}{\alpha} \right)^{1/4} \omega_1, \quad (\text{B.53})$$

so one concludes that the flat directions are given by

$$\begin{pmatrix} \chi \\ \omega_1 \\ \omega_2 \end{pmatrix} = \lambda \begin{pmatrix} \pm \left(\frac{c_0 + c_1\delta^2 + c_2\delta^4}{\alpha} \right)^{1/4} \\ 1 \\ \delta \end{pmatrix}. \quad (\text{B.54})$$

This completes our discussion on the stability of 1-, 2- and 3-vev manifolds and on the classification of the possible flat directions generated by the RG evolution of the quartic couplings. The symmetry breaking patterns occurring in each case identified above are summarised in Table 1.

C A quantitative measure of perturbativity

In this appendix, we develop a method allowing to obtain a quantitative measure of perturbativity based on the comparison of the size of the one- and two-loop contributions to the β -functions. In [51], one of us has proposed a simple perturbativity criterion translating, using definition (E.1), into

$$\left| \beta^{(2)}(g_i) \right| < \frac{1}{2} \left| \beta^{(1)}(g_i) \right|, \quad \forall g_i \quad (\text{C.1})$$

where g_i , $i = 1, \dots, N$ generically denotes all the couplings of the theory. Note that the inclusion of the factor $\frac{1}{2}$ is rather arbitrary, since the boundary (in the space of the couplings of the model) between the perturbative and non-perturbative regimes is anyways equivocal. This being said, the above criterion allows in particular to systematically detect the occurrence of Landau poles in the RG-flow, indicating a breakdown of perturbation theory.

While this criterion was successfully applied in [51] as a way to phenomenologically constrain (extensions of) the SM, it comes with a caveat: A change of sign in the one-loop β -function of any of the couplings systematically violates Eq. (C.1), even in a region of the coupling space where the regime is clearly perturbative. To circumvent this problematic feature, we propose a generalisation of the above criterion simultaneously involving all the couplings of the theory. Letting p be a positive integer and $\alpha > 0$, this generalised perturbativity criterion reads

$$\left(\sum_{i=1}^N \left| \beta^{(2)}(g_i) \right|^p \right)^{1/p} < \alpha \left(\sum_{i=1}^N \left| \beta^{(1)}(g_i) \right|^p \right)^{1/p}, \quad (\text{C.2})$$

or, in a more compact form,

$$\left\| \boldsymbol{\beta}^{(2)}(\mathbf{g}) \right\|_p < \alpha \left\| \boldsymbol{\beta}^{(1)}(\mathbf{g}) \right\|_p, \quad (\text{C.3})$$

where $\|\cdot\|_p$ denotes the usual ℓ_p -norm and where

$$\boldsymbol{\beta}^{(n)}(\mathbf{g}) = \begin{pmatrix} \beta^{(n)}(g_1) \\ \vdots \\ \beta^{(n)}(g_N) \end{pmatrix}. \quad (\text{C.4})$$

The free parameters p and α conveniently allow to adapt the (non-)conservative property of the criterion. As a particular case of (C.3), note that taking $p \rightarrow \infty$ yields

$$\max_i \left| \beta^{(2)}(g_i) \right| < \alpha \max_i \left| \beta^{(1)}(g_i) \right| \quad (\text{C.5})$$

whereas $p = 1$ gives

$$\sum_{i=1}^N \left| \beta^{(2)}(g_i) \right| < \alpha \sum_{i=1}^N \left| \beta^{(1)}(g_i) \right|. \quad (\text{C.6})$$

In a theory with a single coupling g , taking in addition $\alpha = \frac{1}{2}$ in the above expression allows to recover the formula

$$\left| \beta^{(2)}(g) \right| < \frac{1}{2} \left| \beta^{(1)}(g) \right|, \quad (\text{C.7})$$

which coincides with the original criterion (C.1). As a final remark, we have observed that, in practice, the impact of a change in the value of p can be roughly compensated by a change in the value of α . Consequently, in the present analysis we have chosen to fix $p = 1$, therefore using (C.6) as a quantitative measure of the perturbativity of the studied models.

D Scalar potential for the considered models

In this appendix, we provide the expression of the most general (renormalisable) scalar potential for the $\mathbf{10}_H \oplus \mathbf{16}_H \oplus \mathbf{45}_H$ $SO(10)$ model. This will allow us in turn to specialise this expression to the two simplified models considered in this work, where the scalar sector is reduced to $\mathbf{16}_H \oplus \mathbf{45}_H$ and $\mathbf{45}_H$ respectively.

D.1 Definitions and conventions

The fundamental $\mathbf{10}_H$ multiplet is noted H_i in the following. Based on the decomposition

$$\mathbf{10} \otimes \mathbf{10} = \mathbf{54}_S \oplus \mathbf{45}_A \oplus \mathbf{1}, \quad (\text{D.1})$$

the adjoint $\mathbf{45}_H$ field is conveniently expressed as an antisymmetric 10×10 matrix, noted ϕ_{ij} . Finally, reusing the notations from [], the reducible 32-dimensional spinor field is noted Ξ and can be decomposed under $\mathbf{32} = \mathbf{16}_R \oplus \mathbf{16}_L$ as

$$\Xi = \begin{pmatrix} \chi \\ \chi^c \end{pmatrix}. \quad (\text{D.2})$$

The generators of the reducible 32-dimensional representation are given by

$$S_{ij} = \frac{1}{4\sqrt{2}i} [\Gamma_i, \Gamma_j] = \frac{1}{2} \begin{pmatrix} \sigma_{ij} & 0 \\ 0 & \tilde{\sigma}_{ij} \end{pmatrix} \quad (\text{D.3})$$

with $i, j = 1, \dots, 10$. The Γ_i 's are 32×32 matrices satisfying the anticommutation relations

$$\{\Gamma_i, \Gamma_j\} = 2\delta_{ij} \mathbb{1}_{32}, \quad (\text{D.4})$$

characteristic of a Clifford algebra. An explicit form for Γ_i will not be provided here but can be found in []. Note that, as compared to [], an additional factor of $\sqrt{2}$ was included in the denominator of (D.3) (and in the definition of σ_{ij}) in order to match the convention where the Dynkin index of $\mathbf{16}$ equals 2 (instead of 4). Right- and left-handed projectors P_+ and P_- can be constructed such that

$$P_+ \Xi = \begin{pmatrix} \chi \\ 0 \end{pmatrix} \equiv \chi_+, \quad P_- \Xi = \begin{pmatrix} 0 \\ \chi^c \end{pmatrix} \equiv \chi_-. \quad (\text{D.5})$$

We note in passing that the spinor field χ^c is obtained from a conjugation operation

$$\chi^c = C\chi, \quad C \in \mathbf{16}_{SO(10)}, \quad (\text{D.6})$$

characteristic of the discrete left-right symmetry $D \in SO(10)$ referred to as D-parity in the literature []. Finally, it will be useful to construct the auxiliary adjoint fields

$$\Phi_{16} = \frac{1}{4} \sigma_{ij} \phi^{ij} \quad \text{and} \quad \Phi_{32} = \frac{1}{2} S_{ij} \phi^{ij}. \quad (\text{D.7})$$

in order to construct the various gauge invariant operators in a notation adapted to the presence of a scalar spinorial representation.

D.2 Scalar potential for the $\mathbf{10}_H \oplus \mathbf{16}_H \oplus \mathbf{45}_H$ and $\mathbf{45}_H$ models

With the above definitions at hand, we may now write down the most general renormalisable scalar potential built from the scalar representations $\mathbf{10}_H$, $\mathbf{16}_H$ and $\mathbf{45}_H$:

$$\begin{aligned}
V(H, \chi, \phi) = & \mu_1 H_i H^i + \mu_2 \chi^\dagger \chi + \mu_3 \text{Tr}(\Phi_{16}^2) \\
& + \tau_1 (\chi_-^\dagger \Gamma_i \chi_+) H^i + \tau_1^* (\chi_+^\dagger \Gamma_i \chi_-) H^i + \tau_2 \chi^\dagger \Phi_{16} \chi \\
& + \Lambda_1 \text{Tr}(\Phi_{16}^2)^2 + \Lambda_2 \text{Tr}(\Phi_{16}^4) \\
& + \Lambda_3 (H_i H^i)^2 + \Lambda_4 (H_i H^i) \text{Tr}(\Phi_{16}^2) + \Lambda_5 H_i H_j \text{Tr}(\Gamma^i \Phi_{32} \Gamma^j \Phi_{32}) \\
& + \Lambda_6 (\chi^\dagger \chi)^2 + \Lambda_7 (\chi_+^\dagger \Gamma_i \chi_-) (\chi_-^\dagger \Gamma^i \chi_+) + \Lambda_8 (\chi^\dagger \chi) \text{Tr}(\Phi_{16}^2) + \Lambda_9 \chi^\dagger \Phi_{16}^2 \chi \\
& + \Lambda_{10} (H_i H^i) (\chi^\dagger \chi).
\end{aligned} \tag{D.8}$$

It is worth noticing that in the limit $\tau_1 \rightarrow 0$, the above scalar potential is invariant under a global $U(1)$ transformation under which only $\mathbf{16}_H$ is charged¹⁷, *i.e.* under

$$\chi \rightarrow e^{i\alpha} \chi. \tag{D.9}$$

Finally, the $\mathbf{10}_H$ multiplet couples to fermions $\psi \sim \mathbf{16}_F$ through the Yukawa term

$$- \mathcal{L}_Y = Y_{10} (\psi_-^\dagger \Gamma_i \psi_+) H^i + \text{h.c.}, \tag{D.10}$$

where ψ_\pm was defined similarly to χ_\pm (see Eq. (D.5)).

D.3 Scalar potential for the $\mathbf{16}_H \oplus \mathbf{45}_H$ model

We now specialise expression (D.8) to the case of the simplified model considered in this work, where the scalar sector only consists of $\mathbf{16}_H \oplus \mathbf{45}_H$. Discarding in addition the relevant operators in order to achieve scale invariance at the classical level, we write

$$\begin{aligned}
V(\chi, \phi) = & \frac{\lambda_1}{4} \text{Tr}(\Phi_{16}^2)^2 + \lambda_2 \text{Tr}(\Phi_{16}^4) + 4\lambda_6 (\chi^\dagger \chi)^2 + \lambda_7 (\chi_+^\dagger \Gamma_i \chi_-) (\chi_-^\dagger \Gamma^i \chi_+) \\
& + 2\lambda_8 (\chi^\dagger \chi) \text{Tr}(\Phi_{16}^2) + 8\lambda_9 \chi^\dagger \Phi_{16}^2 \chi.
\end{aligned} \tag{D.11}$$

We note that the normalisation of the various operators is arbitrary and that the six quartic couplings λ_i were defined such that perturbativity is lost around $\lambda_i \gtrsim 1$. Our notation and conventions translate to those of [5, 21, 47] according to:

$$\lambda_1 \leftrightarrow 4a_1, \quad \lambda_2 \leftrightarrow a_2, \quad \lambda_6 \leftrightarrow \frac{\lambda_1}{16}, \quad \lambda_7 \leftrightarrow \frac{\lambda_2}{4}, \quad \lambda_8 \leftrightarrow \alpha, \quad \lambda_9 \leftrightarrow \frac{\beta}{4}. \tag{D.12}$$

Following the comment made above, the absence of relevant operators in (D.11) implies invariance under the $U(1)$ global symmetry (D.9). Finally, the scalar potential for the $\mathbf{45}_H$ model simply reads

$$V(\phi) = \frac{\lambda_1}{4} \text{Tr}(\Phi_{16}^2)^2 + \lambda_2 \text{Tr}(\Phi_{16}^4). \tag{D.13}$$

¹⁷Note that this global symmetry could be restored for $\tau_1 \neq 0$ by complexifying and assigning a $U(1)$ charge to the $\mathbf{10}_H$ multiplet. Invariance of the Yukawa term (D.10) would in turn require to give a charge to the fermionic $\mathbf{16}_F$ multiplet.

E β -functions

The β -functions for the couplings of the three models presented in the previous section were computed up to the two-loop level using the tool PyR@TE 3 [16]. We report here the obtained expressions, first in the case of the $\mathbf{10}_H \oplus \mathbf{16}_H \oplus \mathbf{45}_H$ model¹⁸, then in the case of the simplified $\mathbf{16}_H \oplus \mathbf{45}_H$ model. In the following, we use the convention

$$\beta(X) \equiv \mu \frac{dX}{d\mu} \equiv \frac{1}{(4\pi)^2} \beta^{(1)}(X) + \frac{1}{(4\pi)^4} \beta^{(2)}(X). \quad (\text{E.1})$$

E.1 $\mathbf{10}_H \oplus \mathbf{16}_H \oplus \mathbf{45}_H$ model

We provide below the one-loop β -functions for the full $\mathbf{10}_H \oplus \mathbf{16}_H \oplus \mathbf{45}_H$ model.

Gauge coupling.

$$\beta^{(1)}(g) = -\frac{139}{6}g^3 \quad (\text{E.2})$$

Yukawa coupling.

$$\beta^{(1)}(Y_{10}) = -24Y_{10}Y_{10}^*Y_{10} + 64 \text{Tr}(Y_{10}Y_{10}^*)Y_{10} - \frac{135}{4}g^2Y_{10} \quad (\text{E.3})$$

Quartic couplings.

$$\begin{aligned} \beta^{(1)}(\Lambda_1) = & 1696\Lambda_1^2 + 412\Lambda_1\Lambda_2 + \frac{279}{8}\Lambda_2^2 + 20\Lambda_4^2 + 48\Lambda_4\Lambda_5 + 112\Lambda_5^2 + 64\Lambda_8^2 \\ & + 4\Lambda_8\Lambda_9 - 96\Lambda_1g^2 + \frac{27}{16}g^4 \end{aligned} \quad (\text{E.4})$$

$$\beta^{(1)}(\Lambda_2) = 384\Lambda_1\Lambda_2 - 4\Lambda_2^2 - 512\Lambda_5^2 + \Lambda_9^2 - 96\Lambda_2g^2 - 3g^4 \quad (\text{E.5})$$

$$\begin{aligned} \beta^{(1)}(\Lambda_3) = & 144\Lambda_3^2 + 360\Lambda_4^2 + 864\Lambda_4\Lambda_5 + 1440\Lambda_5^2 + 16\Lambda_{10}^2 - 54\Lambda_3g^2 + \frac{27}{8}g^4 \\ & + 256\Lambda_3 \text{Tr}(Y_{10}Y_{10}^*) - 256 \text{Tr}(Y_{10}Y_{10}^*Y_{10}Y_{10}^*) \end{aligned} \quad (\text{E.6})$$

$$\begin{aligned} \beta^{(1)}(\Lambda_4) = & 1504\Lambda_1\Lambda_4 + 1728\Lambda_1\Lambda_5 + 206\Lambda_2\Lambda_4 + 276\Lambda_2\Lambda_5 + 96\Lambda_3\Lambda_4 + 96\Lambda_3\Lambda_5 \\ & + 32\Lambda_4^2 + 768\Lambda_5^2 + 64\Lambda_{10}\Lambda_8 + 2\Lambda_{10}\Lambda_9 - 75\Lambda_4g^2 + \frac{15}{8}g^4 \\ & + 128\Lambda_4 \text{Tr}(Y_{10}Y_{10}^*) \end{aligned} \quad (\text{E.7})$$

$$\begin{aligned} \beta^{(1)}(\Lambda_5) = & 64\Lambda_1\Lambda_5 - 24\Lambda_2\Lambda_5 + 16\Lambda_3\Lambda_5 + 64\Lambda_4\Lambda_5 - 192\Lambda_5^2 - 75\Lambda_5g^2 - \frac{9}{16}g^4 \\ & + 128\Lambda_5 \text{Tr}(Y_{10}Y_{10}^*) \end{aligned} \quad (\text{E.8})$$

$$\begin{aligned} \beta^{(1)}(\Lambda_6) = & 80\Lambda_6^2 + 160\Lambda_6\Lambda_7 + 320\Lambda_7^2 + 1440\Lambda_8^2 + 90\Lambda_8\Lambda_9 + \frac{105}{32}\Lambda_9^2 + 20\Lambda_{10}^2 \\ & - \frac{135}{2}\Lambda_6g^2 + \frac{315}{32}g^4 \end{aligned} \quad (\text{E.9})$$

$$\beta^{(1)}(\Lambda_7) = 24\Lambda_6\Lambda_7 + \frac{3}{8}\Lambda_9^2 - \frac{135}{2}\Lambda_7g^2 + \frac{9}{8}g^4 \quad (\text{E.10})$$

¹⁸Although this model was not studied in the present work, we provide the corresponding set of β -functions since we believe that these might be useful to the reader.

$$\begin{aligned}
\beta^{(1)}(\Lambda_8) &= 1504\Lambda_1\Lambda_8 + 45\Lambda_1\Lambda_9 + 206\Lambda_2\Lambda_8 + \frac{93}{16}\Lambda_2\Lambda_9 + 68\Lambda_6\Lambda_8 + 2\Lambda_6\Lambda_9 \\
&\quad + 80\Lambda_7\Lambda_8 + 2\Lambda_7\Lambda_9 + 32\Lambda_8^2 + \frac{3}{8}\Lambda_9^2 + 20\Lambda_{10}\Lambda_4 + 24\Lambda_{10}\Lambda_5 \\
&\quad - \frac{327}{4}\Lambda_8g^2 + \frac{9}{8}g^4
\end{aligned} \tag{E.11}$$

$$\begin{aligned}
\beta^{(1)}(\Lambda_9) &= 64\Lambda_1\Lambda_9 + 20\Lambda_2\Lambda_9 + 4\Lambda_6\Lambda_9 + 16\Lambda_7\Lambda_9 + 64\Lambda_8\Lambda_9 + 17\Lambda_9^2 \\
&\quad - \frac{327}{4}\Lambda_9g^2 + 12g^4
\end{aligned} \tag{E.12}$$

$$\begin{aligned}
\beta^{(1)}(\Lambda_{10}) &= 1440\Lambda_4\Lambda_8 + 45\Lambda_4\Lambda_9 + 1728\Lambda_5\Lambda_8 + 54\Lambda_5\Lambda_9 + 96\Lambda_{10}\Lambda_3 + 68\Lambda_{10}\Lambda_6 \\
&\quad + 80\Lambda_{10}\Lambda_7 + 8\Lambda_{10}^2 - \frac{243}{4}\Lambda_{10}g^2 + \frac{27}{8}g^4 + 128\Lambda_{10} \text{Tr}(Y_{10}Y_{10}^*)
\end{aligned} \tag{E.13}$$

Scalar mass and cubic couplings.

$$\begin{aligned}
\beta^{(1)}(\mu_1) &= 96\Lambda_3\mu_1 + 32\Lambda_{10}\mu_2 + 720\Lambda_4\mu_3 + 864\Lambda_5\mu_3 - 27g^2\mu_1 \\
&\quad + 128\mu_1 \text{Tr}(Y_{10}Y_{10}^*) + 64|\tau_1|^2
\end{aligned} \tag{E.14}$$

$$\begin{aligned}
\beta^{(1)}(\mu_2) &= \frac{45}{4}\tau_2^2 + 40\Lambda_{10}\mu_1 + 68\Lambda_6\mu_2 + 80\Lambda_7\mu_2 + 1440\Lambda_8\mu_3 + 45\Lambda_9\mu_3 \\
&\quad - \frac{135}{4}g^2\mu_2 + 80|\tau_1|^2
\end{aligned} \tag{E.15}$$

$$\begin{aligned}
\beta^{(1)}(\mu_3) &= 40\Lambda_4\mu_1 + 48\Lambda_5\mu_1 + 64\Lambda_8\mu_2 + 2\Lambda_9\mu_2 + 1504\Lambda_1\mu_3 + 206\Lambda_2\mu_3 \\
&\quad - 48g^2\mu_3 + \tau_2^2
\end{aligned} \tag{E.16}$$

$$\beta^{(1)}(\tau_1) = 4\Lambda_6\tau_1 + 64\Lambda_7\tau_1 + 8\Lambda_{10}\tau_1 - \frac{189}{4}g^2\tau_1 + 64\tau_1 \text{Tr}(Y_{10}Y_{10}^*) \tag{E.17}$$

$$\beta^{(1)}(\tau_2) = 4\Lambda_6\tau_2 - 48\Lambda_7\tau_2 + 32\Lambda_8\tau_2 + 29\Lambda_9\tau_2 - \frac{231}{4}g^2\tau_2 \tag{E.18}$$

E.2 $16_H \oplus 45_H$ and 45_H models

We provide below the β -functions for the simplified $16_H \oplus 45_H$ model up to the two-loop level, the two-loop contributions being used in the present analysis to establish a quantitative measure of perturbativity (see Appendix C).

Gauge coupling.

$$\beta^{(1)}(g) = -\frac{70}{3}g^3 \tag{E.19}$$

Quartic couplings.

$$\beta^{(1)}(\lambda_1) = 424\lambda_1^2 + 412\lambda_1\lambda_2 + \frac{279}{2}\lambda_2^2 + 256\lambda_8^2 + 128\lambda_8\lambda_9 - 96g^2\lambda_1 + \frac{27}{4}g^4 \tag{E.20}$$

$$\beta^{(1)}(\lambda_2) = 96\lambda_1\lambda_2 - 4\lambda_2^2 + 64\lambda_9^2 - 96g^2\lambda_2 - 3g^4 \tag{E.21}$$

$$\begin{aligned}
\beta^{(1)}(\lambda_6) &= 320\lambda_6^2 + 160\lambda_6\lambda_7 + 80\lambda_7^2 + 360\lambda_8^2 + 180\lambda_8\lambda_9 + \frac{105}{2}\lambda_9^2 \\
&\quad - \frac{135}{2}g^2\lambda_6 + \frac{315}{128}g^4
\end{aligned} \tag{E.22}$$

$$\beta^{(1)}(\lambda_7) = 96\lambda_6\lambda_7 + 24\lambda_9^2 - \frac{135}{2}g^2\lambda_7 + \frac{9}{8}g^4 \quad (\text{E.23})$$

$$\begin{aligned} \beta^{(1)}(\lambda_8) = & 376\lambda_1\lambda_8 + 90\lambda_1\lambda_9 + 206\lambda_2\lambda_8 + \frac{93}{2}\lambda_2\lambda_9 + 272\lambda_6\lambda_8 + 64\lambda_6\lambda_9 + 80\lambda_7\lambda_8 \\ & + 16\lambda_7\lambda_9 + 32\lambda_8^2 + 24\lambda_9^2 - \frac{327}{4}g^2\lambda_8 + \frac{9}{8}g^4 \end{aligned} \quad (\text{E.24})$$

$$\begin{aligned} \beta^{(1)}(\lambda_9) = & 16\lambda_1\lambda_9 + 20\lambda_2\lambda_9 + 16\lambda_6\lambda_9 + 16\lambda_7\lambda_9 + 64\lambda_8\lambda_9 + 136\lambda_9^2 \\ & - \frac{327}{4}g^2\lambda_9 + \frac{3}{2}g^4 \end{aligned} \quad (\text{E.25})$$

The β -functions of $\lambda_{1,2}$ in the case of the 45_H -only model are simply found by taking the limit $\lambda_{6,7,8,9} \rightarrow 0$ in the above expressions. Note however that the gauge coupling β -function reduces to

$$\beta^{(1)}(g) = -24g^3. \quad (\text{E.26})$$

References

- [1] H. Georgi and S.L. Glashow, Unity of all elementary-particle forces, [Phys. Rev. Lett.](#) **32** (1974) 438.
- [2] H. Fritzsch and P. Minkowski, Unified Interactions of Leptons and Hadrons, [Annals Phys.](#) **93** (1975) 193.
- [3] A.J. Buras, J.R. Ellis, M.K. Gaillard and D.V. Nanopoulos, Aspects of the Grand Unification of Strong, Weak and Electromagnetic Interactions, [Nucl. Phys. B](#) **135** (1978) 66.
- [4] J.C. Baez and J. Huerta, The Algebra of Grand Unified Theories, [Bull. Am. Math. Soc.](#) **47** (2010) 483 [[0904.1556](#)].
- [5] L. Di Luzio, Aspects of symmetry breaking in Grand Unified Theories, Ph.D. thesis, SISSA, Trieste, 2011. [1110.3210](#).
- [6] S. Bertolini, L. Di Luzio and M. Malinsky, Seesaw Scale in the Minimal Renormalizable SO(10) Grand Unification, [Phys. Rev. D](#) **85** (2012) 095014 [[1202.0807](#)].
- [7] M. Yoshimura, Unified Gauge Theories and the Baryon Number of the Universe, [Phys. Rev. Lett.](#) **41** (1978) 281.
- [8] A.Y. Ignatiev, V.A. Kuzmin and M.E. Shaposhnikov, Baryon Asymmetry of the Universe in Grand Unified Theories, [Phys. Lett. B](#) **87** (1979) 114.
- [9] V.A. Kuzmin and M.E. Shaposhnikov, Baryon Asymmetry of the Universe Versus Left-right Symmetry, [Phys. Lett. B](#) **92** (1980) 115.
- [10] A. Eichhorn, A. Held and C. Wetterich, Quantum-gravity predictions for the fine-structure constant, [Phys. Lett. B](#) **782** (2018) 198 [[1711.02949](#)].
- [11] A. Eichhorn, A. Held and C. Wetterich, Predictive power of grand unification from quantum gravity, [JHEP](#) **08** (2020) 111 [[1909.07318](#)].

- [12] V. Braun, Y.-H. He, B.A. Ovrut and T. Pantev, A Heterotic standard model, [*Phys. Lett. B* **618** \(2005\) 252](#) [[hep-th/0501070](#)].
- [13] L.B. Anderson, J. Gray, D. Grayson, Y.-H. He and A. Lukas, Yukawa Couplings in Heterotic Compactification, [*Commun. Math. Phys.* **297** \(2010\) 95](#) [[0904.2186](#)].
- [14] M. McGuigan, Dark Horse, Dark Matter: Revisiting the $SO(16) \times SO(16)$ Nonsupersymmetric Model in the LHC and Dark Energy, [1907.01944](#).
- [15] L.B. Anderson, J. Gray, M. Larfors, M. Magill and R. Schneider, Generalized Vanishing Theorems for Yukawa Couplings in Heterotic Compactifications, [2103.10454](#).
- [16] L. Sartore and I. Schienbein, PyR@TE 3, [*Comput. Phys. Commun.* **261** \(2021\) 107819](#) [[2007.12700](#)].
- [17] L. Chataignier, T. Prokopec, M.G. Schmidt and B. Swiezewska, Single-scale Renormalisation Group Improvement of Multi-scale Effective Potentials, [*JHEP* **03** \(2018\) 014](#) [[1801.05258](#)].
- [18] K. Kannike, K. Loos and L. Marzola, Minima of classically scale-invariant potentials, [*JHEP* **06** \(2021\) 128](#) [[2011.12304](#)].
- [19] T. Ohlsson, M. Pernow and E. Sönnerlind, Realizing unification in two different $SO(10)$ models with one intermediate breaking scale, [*Eur. Phys. J. C* **80** \(2020\) 1089](#) [[2006.13936](#)].
- [20] B. Bajc, A. Melfo, G. Senjanovic and F. Vissani, Yukawa sector in non-supersymmetric renormalizable $SO(10)$, [*Phys. Rev. D* **73** \(2006\) 055001](#) [[hep-ph/0510139](#)].
- [21] S. Bertolini, L. Di Luzio and M. Malinsky, On the vacuum of the minimal nonsupersymmetric $SO(10)$ unification, [*Phys. Rev. D* **81** \(2010\) 035015](#) [[0912.1796](#)].
- [22] S. Bertolini, L. Di Luzio and M. Malinsky, Intermediate mass scales in the non-supersymmetric $SO(10)$ grand unification: A Reappraisal, [*Phys. Rev.* **D80** \(2009\) 015013](#) [[0903.4049](#)].
- [23] M.E. Machacek and M.T. Vaughn, Two Loop Renormalization Group Equations in a General Quantum Field Theory. 1. Wave Function Renormalization, [*Nucl. Phys. B* **222** \(1983\) 83](#).
- [24] M.E. Machacek and M.T. Vaughn, Two Loop Renormalization Group Equations in a General Quantum Field Theory. 2. Yukawa Couplings, [*Nucl. Phys. B* **236** \(1984\) 221](#).
- [25] M.E. Machacek and M.T. Vaughn, Two Loop Renormalization Group Equations in a General Quantum Field Theory. 3. Scalar Quartic Couplings, [*Nucl. Phys. B* **249** \(1985\) 70](#).
- [26] I. Schienbein, F. Staub, T. Steudtner and K. Svirina, Revisiting RGEs for general gauge theories, [*Nucl. Phys. B* **939** \(2019\) 1](#) [[1809.06797](#)].

- [27] C. Poole and A.E. Thomsen,
Constraints on 3- and 4-loop β -functions in a general four-dimensional Quantum Field Theory, [JHEP **09** \(2019\) 055](#) [[1906.04625](#)].
- [28] L. Sartore,
General renormalization group equations for dimensionful couplings in the $\overline{\text{MS}}$ scheme, [Phys. Rev. D **102** \(2020\) 076002](#) [[2006.12307](#)].
- [29] M.B. Einhorn and D.R.T. Jones,
A NEW RENORMALIZATION GROUP APPROACH TO MULTISCALE PROBLEMS, [Nucl. Phys. B **230** \(1984\) 261](#).
- [30] M. Bando, T. Kugo, N. Maekawa and H. Nakano,
Improving the effective potential: Multimass scale case, [Prog. Theor. Phys. **90** \(1993\) 405](#) [[hep-ph/9210229](#)].
- [31] C. Ford, D.R.T. Jones, P.W. Stephenson and M.B. Einhorn,
The Effective potential and the renormalization group, [Nucl. Phys. B **395** \(1993\) 17](#) [[hep-lat/9210033](#)].
- [32] C. Ford, Multiscale renormalization group improvement of the effective potential, [Phys. Rev. D **50** \(1994\) 7531](#) [[hep-th/9404085](#)].
- [33] C. Ford and C. Wiesendanger,
A Multiscale subtraction scheme and partial renormalization group equations in the $O(N)$ symmetric ϕ^4 theory, [Phys. Rev. D **55** \(1997\) 2202](#) [[hep-ph/9604392](#)].
- [34] C. Ford and C. Wiesendanger, Multiscale renormalization, [Phys. Lett. B **398** \(1997\) 342](#) [[hep-th/9612193](#)].
- [35] J.A. Casas, V. Di Clemente and M. Quiros,
The Effective potential in the presence of several mass scales, [Nucl. Phys. B **553** \(1999\) 511](#) [[hep-ph/9809275](#)].
- [36] T.G. Steele, Z.-W. Wang and D.G.C. McKeon,
Multiscale renormalization group methods for effective potentials with multiple scalar fields, [Phys. Rev. D **90** \(2014\) 105012](#) [[1409.3489](#)].
- [37] L. Chataignier, T. Prokopec, M.G. Schmidt and B. Świeżewska,
Systematic analysis of radiative symmetry breaking in models with extended scalar sector, [JHEP **08** \(2018\) 083](#) [[1805.09292](#)].
- [38] E. Gildener and S. Weinberg, Symmetry Breaking and Scalar Bosons, [Phys. Rev. D **13** \(1976\) 3333](#).
- [39] M. Yasuè, Symmetry breaking of $so(10)$ and constraints on the higgs potential: Adjoint 45 and spinorial 16 representations, [Phys. Rev. D **24** \(1981\) 1005](#).
- [40] M. Yasue,
HOW TO BREAK $SO(10)$ VIA $SO(4) \times SO(6)$ DOWN TO $SU(2)(L) \times SU(3)(C) \times U(1)$, [Phys. Lett. B **103** \(1981\) 33](#).
- [41] G. Anastaze, J.P. Derendinger and F. Buccella,
INTERMEDIATE SYMMETRIES IN THE $SO(10)$ MODEL WITH $(16+16) + 45$ HIGGSSES, [Z. Phys. C **20** \(1983\) 269](#).

- [42] K.S. Babu and E. Ma, Symmetry Breaking in SO(10): Higgs Boson Structure, [Phys. Rev. D](#) **31** (1985) 2316.
- [43] S. Bertolini, L. Di Luzio and M. Malinsky, Towards a New Minimal SO(10) Unification, [AIP Conf. Proc.](#) **1467** (2012) 37 [[1205.5637](#)].
- [44] J. Kim, General Method for Analyzing Higgs Potentials, [Nucl. Phys. B](#) **196** (1982) 285.
- [45] G. Sartori and G. Valente, Allowed and observable phases in two Higgs doublet standard models, [hep-ph/0304026](#).
- [46] G. Sartori and G. Valente, Symmetry allowed, but unobservable, phases in renormalizable gauge field theory models, [hep-th/0405021](#).
- [47] S. Bertolini, L. Di Luzio and M. Malinsky, The quantum vacuum of the minimal SO(10) GUT, [J. Phys. Conf. Ser.](#) **259** (2010) 012098 [[1010.0338](#)].
- [48] L.-F. Li, Group Theory of the Spontaneously Broken Gauge Symmetries, [Phys. Rev. D](#) **9** (1974) 1723.
- [49] A. Held, J.H. Kwapisz and L. Sartore. to appear, 2021.
- [50] M. Yasue, Symmetry Breaking of SO(10) and Constraints on Higgs Potential. 1. Adjoint (45) and Spinorial (16), [Phys. Rev. D](#) **24** (1981) 1005.
- [51] A. Held, Effective asymptotic safety and its predictive power: Gauge-Yukawa theories, [Front. in Phys.](#) **8** (2020) 341 [[2003.13642](#)].
- [52] K. Jarkovská, M. Malinský, T. Mede and V. Susič, Quantum guts of the minimal potentially realistic SO(10) Higgs model, [2109.06784](#).
- [53] W.H. Press, B.S. Ryden and D.N. Spergel, Dynamical Evolution of Domain Walls in an Expanding Universe, [Astrophys. J.](#) **347** (1989) 590.
- [54] D. Coulson, Z. Lalak and B.A. Ovrut, Biased domain walls, [Phys. Rev. D](#) **53** (1996) 4237.
- [55] Z. Lalak, S. Lola, B.A. Ovrut and G.G. Ross, Large scale structure from biased nonequilibrium phase transitions: Percolation theory picture, [Nucl. Phys. B](#) **434** (1995) 675 [[hep-ph/9404218](#)].
- [56] T. Krajewski, J.H. Kwapisz, Z. Lalak and M. Lewicki, Stability of domain walls in models with asymmetric potentials, [2103.03225](#).
- [57] A. Salvio and A. Strumia, Agravity, [JHEP](#) **06** (2014) 080 [[1403.4226](#)].
- [58] V. Braun, Y.-H. He, B.A. Ovrut and T. Pantev, A Standard model from the E(8) x E(8) heterotic superstring, [JHEP](#) **06** (2005) 039 [[hep-th/0502155](#)].
- [59] V. Braun, Y.-H. He and B.A. Ovrut, Yukawa couplings in heterotic standard models, [JHEP](#) **04** (2006) 019 [[hep-th/0601204](#)].

- [60] L.B. Anderson, J. Gray, D. Grayson, Y.-H. He and A. Lukas, Yukawa Couplings in Heterotic Compactification, [Commun. Math. Phys.](#) **297** (2010) 95 [[0904.2186](#)].
- [61] D. Tong, [String Theory](#), [0908.0333](#).
- [62] E.L. Rees, Graphical discussion of the roots of a quartic equation, [The American Mathematical Monthly](#) **29** (1922) 51.
- [63] D. Lazard, Quantifier elimination: Optimal solution for two classical examples, [Journal of Symbolic Computation](#) **5** (1988) 261.
- [64] K. Kannike, Vacuum Stability of a General Scalar Potential of a Few Fields, [Eur. Phys. J. C](#) **76** (2016) 324 [[1603.02680](#)].